

Article

Produced Gas and Condensate Geochemistry of the Marcellus Formation in the Appalachian Basin: Insights into Petroleum Maturity, Migration, and Alteration in an Unconventional Shale Reservoir

Christopher D. Laughrey

Stratum Reservoir, Geochemical Interpretive Services, Evergreen, CO 80439, USA;
christopher.laughrey@stratumreservoir.com

Abstract: The Middle Devonian Marcellus Formation of North America is the most prolific hydrocarbon play in the Appalachian basin, the second largest producer of natural gas in the United States, and one of the most productive gas fields in the world. Regional differences in Marcellus fluid chemistry reflect variations in thermal maturity, migration, and hydrocarbon alteration. These differences define specific wet gas/condensate and dry gas production in the basin. Marcellus gases co-produced with condensate in southwest Pennsylvania and northwest West Virginia are mixtures of residual primary-associated gases generated in the late oil window and postmature secondary hydrocarbons generated from oil cracking in the wet gas window. Correlation of API gravity and C₇ expulsion temperatures, high heptane and isoheptane ratios, and the gas geochemical data confirm that the Marcellus condensates formed through oil cracking. Respective low toluene/nC₇ and high nC₇/methylcyclohexane ratios indicate selective depletion of low-boiling point aromatics and cyclic light saturates in all samples, suggesting that water washing and gas stripping altered the fluids. These alterations may be related to deep migration of hot basinal brines. Dry Marcellus gases produced in northeast Pennsylvania and northcentral West Virginia are mixtures of overmature methane largely cracked from refractory kerogen and ethane and propane cracked from light oil and wet gas. Carbon and hydrogen isotope distributions are interpreted to indicate (1) mixing of hydrocarbons of different thermal maturities, (2) high temperature Rayleigh fractionation of wet gas during redox reactions with transition metals and formation water, (3) isotope exchange between methane and water, and, possibly, (4) thermodynamic equilibrium conditions within the reservoirs. Evidence for thermodynamic equilibrium in the dry gases includes measured molecular proportions (C₁/(C₁ – C₅) = 0.96 to 0.985) and δ¹³C₁ values significantly greater than δ¹³C_{KEROGEN}. Noble gas systematics support the interpretation of hydrocarbon–formation water interactions, constrain the high thermal maturity of the hydrocarbon fluids, and provide a method of quantifying gas retention versus expulsion in the reservoirs.



Citation: Laughrey, C.D. Produced Gas and Condensate Geochemistry of the Marcellus Formation in the Appalachian Basin: Insights into Petroleum Maturity, Migration, and Alteration in an Unconventional Shale Reservoir. *Minerals* **2022**, *12*, 1222. <https://doi.org/10.3390/min12101222>

Academic Editor: Luca Aldega

Received: 16 June 2022

Accepted: 15 September 2022

Published: 27 September 2022

Publisher's Note: MDPI stays neutral with regard to jurisdictional claims in published maps and institutional affiliations.

Keywords: late oil window; postmature and overmature kerogen; primary and secondary hydrocarbons; hydrocarbon isotopes and isotope reversals; C₇ hydrocarbon analysis; water washing; gas stripping; noble gases



Copyright: © 2022 by the author. Licensee MDPI, Basel, Switzerland. This article is an open access article distributed under the terms and conditions of the Creative Commons Attribution (CC BY) license (<https://creativecommons.org/licenses/by/4.0/>).

1. Introduction

The Middle Devonian Marcellus Formation in the Appalachian basin of North America is an iconic stratigraphic interval. It is the most prolific hydrocarbon play in the basin, the second largest producer of natural gas in the United States, and, in combination with the Ordovician Utica shale, the largest source of natural gas and natural gas liquids (NGL) in the world [1,2]. Proven natural gas reserves for the Marcellus Formation total more than 129 tcf and proven lease condensate reserves total 247 million barrels [3]. The Marcellus is also a prospective CO₂ sequestration reservoir and a potential seal for Carbon Capture

and Underground Storage (CCUS) and NGL storage [4,5]. It is a potential source of critical minerals [6]. In contrast to its natural resource utility, the Marcellus is a potential source of stray gas contamination in ground water supplies and building structures as well as fugitive emissions of atmospheric methane [7–10].

Several critical geologic factors define the Marcellus play in the Appalachian basin. These factors are thermal maturity, pressure, thickness, porosity and permeability, gas-in-place, natural fracturing, mineralogy, depth, structural setting, rock mechanics, target landing issues, diagenesis, and hydrocarbon alteration [11–13]. Thermal maturity appears to define specific wet gas and dry gas production in the Appalachian basin [1] (Figure 1). Condensate production occurs in the western part of the basin where wet gases with approximately 1400 MMBtu/Mcf are recovered from reservoir depths of –1067 to –1524 m (–3500 to –5000 ft.) subsea with reported vitrinite reflectance (VR_o) of 1.0 to 2.8%. Dry gas with 1000 to 1080 MMBtu/Mcf is produced from reservoir depths of approximately –914 to –1981 m (–3000 to –6500 ft.) subsea with reported VR_o from 2.0 to >3.0%.

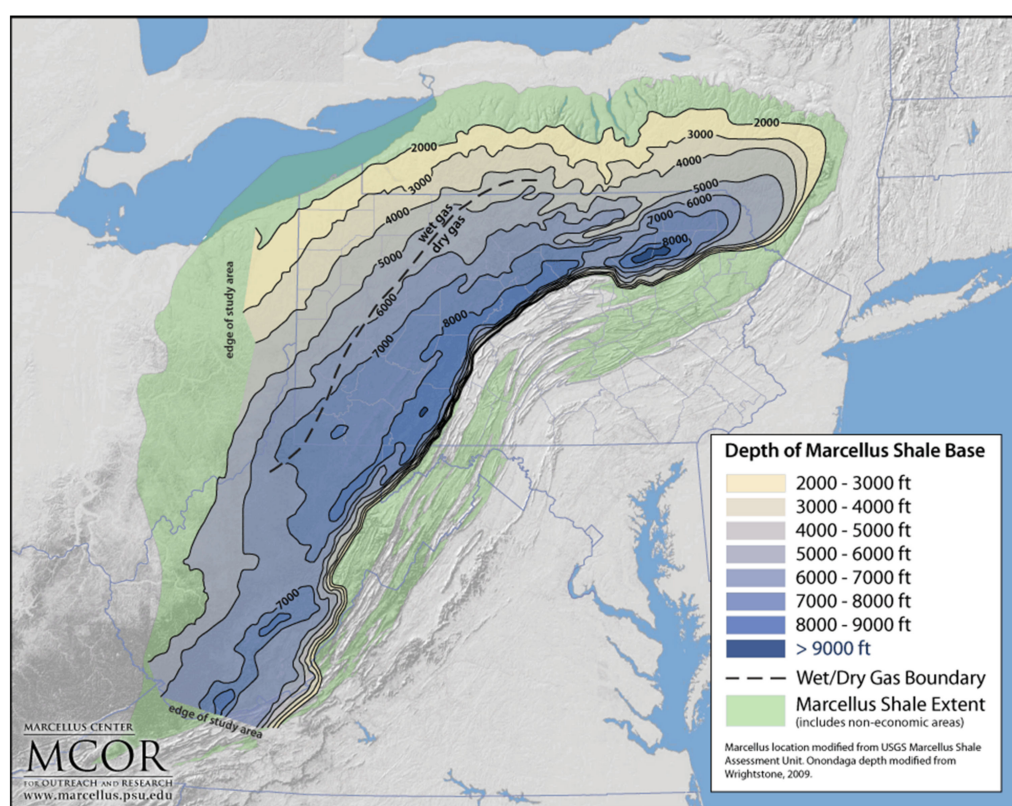


Figure 1. Map showing regional distribution of wet gas and dry gas produced from the Marcellus Formation in the Appalachian basin. Contours are depth in feet to the base of the Marcellus. Downloaded from the Pennsylvania State University Marcellus Center for Outreach and Research, <http://www.marcellus.psu.edu/resources/images/wet-dry--line--with--depth.gif>. (Accessed on 6 April 2022).

In this contribution, integrated from twenty-four years of study of Marcellus natural gas/condensate chemical and isotope data, I argue that regional differences in fluid chemistry reflect variations in thermal maturity, hydrocarbon alteration, and geological processes active in the petroleum system. These differences not only define specific wet gas and dry gas production in the basin BUT predict relative productivity as well. Marcellus Formation hydrocarbon composition, isotope, and noble gas geochemistry provide a quantitative methodology independent of rock data, choke management, and completion design for defining and mapping economic production limits. Noble gas systematics provide a method of quantifying hydrocarbon maturity and gas retention versus fluid expulsion or

loss from the reservoirs. The data and geochemical trends documented in this report can also facilitate the identification of sources of stray gas contamination and provide fundamental baseline measurements for comparison with data derived from recent atmospheric measurements conducted to monitor fugitive emissions of atmospheric methane [7–10].

2. Geological Framework and Current Status of Marcellus Formation Research

The Appalachian basin and its foreland represent mountain building throughout most of the Paleozoic on the former eastern convergent margin of North America [14]. The Devonian Appalachian basin was a retroarc foreland basin that developed adjacent to the Acadian orogenic belt, a mountain chain built by oblique collision of the North American continental margin with Avalon terrane [14–17]. Crustal loading by the resultant fold and thrust belt caused subsidence of an elongate foreland basin which was mostly filled with siliciclastic sediments eroded from the uplifted orogen. Sediment supply from the uplifting and eroding Appalachian Mountains generally exceeded subsidence during the late Devonian Acadian and Pennsylvanian-Permian Alleghenian orogenies resulting in mostly clastic terrestrial deposits that spread across the basin and foreland in a broad, westward coalescing coastal plain [18]. Periods of high eustasy and/or reduced sediment supply resulted in marine incursions and both clastic and carbonate deposition across the region. The consequent Middle to Upper Devonian sedimentary section comprises the Catskill Delta succession of which the Marcellus Formation is an important component [19] (Figure 2).

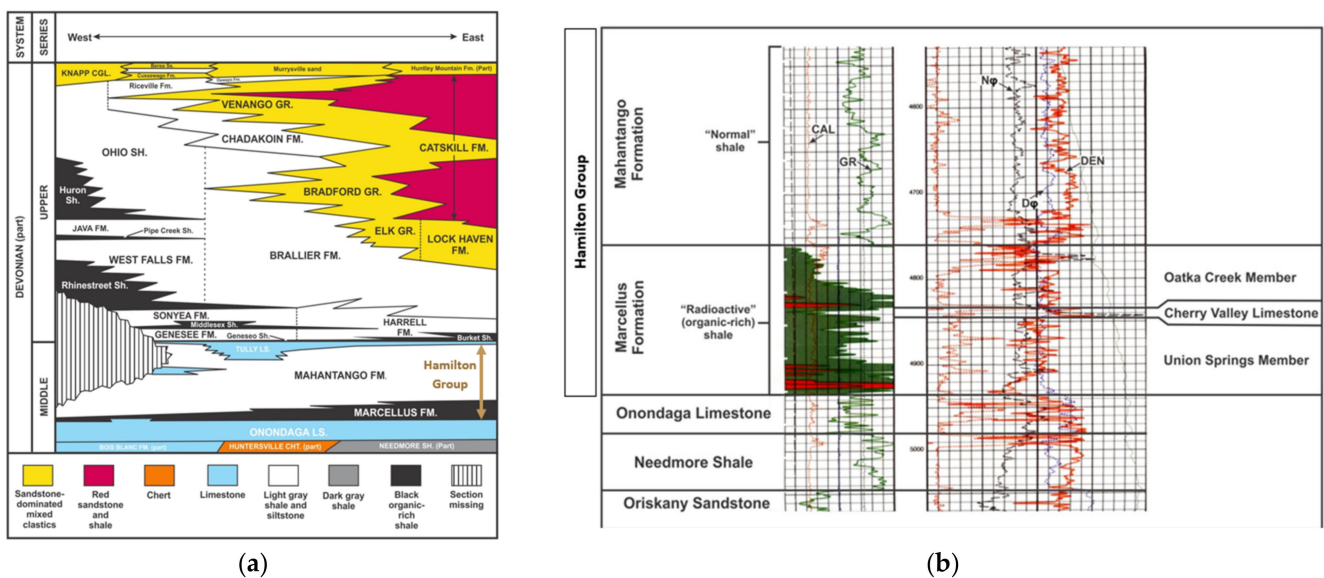


Figure 2. (a) Correlation diagram of Middle and Upper Devonian stratigraphic intervals in western and north-central Pennsylvania. From Carter et al. [20]. Also see Harper et al. [21] and Carter [22]. Stratigraphic units above the Middle Devonian Onondaga Limestone comprise the siliciclastic successions of the Catskill Delta. FM.—Formation; SH—Shale; GR—Group; LS—Limestone; CHT—Chert. (b) Diagram of parts of a wireline geophysical log showing the stratigraphic nomenclature for the Marcellus Formation in the subsurface of Pennsylvania. From Carter et al. [20]. CAL—Caliper; GR—Gamma Ray; DEN—Bulk Density; NØ—Neutron Porosity; DØ—Density Porosity.

The Marcellus Formation includes the oldest of a dozen or so regionally extensive organic-rich petroliferous black shale deposits associated with the Catskill delta in eastern North America [23]. The Marcellus Formation is the basal unit of the Hamilton Group (Figure 2). It is about 305 m (1000 ft.) thick in central Pennsylvania, but thins to the north, the west, and the south and feathers out of the sequence in the subsurface of eastern Ohio, western West Virginia, and southwestern Virginia [23]. Throughout much of the basin, the Marcellus Formation comprises two black shale members separated by a sequence

of limestone, shale, and lesser sandstone of variable thickness [24] (Figure 2). In eastern West Virginia, however, these two shale members are only mappable to the point where the medial Cherry Valley Member limestone can be recognized [25]. The Cherry Valley Member then becomes very thin and loosely defined moving from northeast to southwest across most of West Virginia [25]. The Marcellus Formation encompasses two third-order transgressive–regressive sequences, the thicknesses of which reflect the interplay of Acadian thrust-load-induced subsidence, short-term base-level fluctuations, and recurrent basement tectonics [24]. Sea-level changes, which influenced clastic dilution and organic carbon production and preservation, were the principal control for organic matter accumulation in the black shales [26]. Sea-level rise led to sediment starvation and organic carbon concentration in distal basin sediments.

Marcellus Formation reservoir shales are dominated by nine principal mineral phases including quartz, muscovite, illite, pyrite, chlorite, albite, calcite, dolomite, and barite [12,27]. Variable amounts of anhydrite, kaolinite, and apatite are reported in some cores [12]. Four distinct mineralogical facies within the Marcellus shales reflect depositional influences on the variability of total organic carbon (TOC) between the upper and lower black shale members [27]. The medial Cherry Valley Member limestones contrast lithologically and petrophysically with the bounding organic-rich shales and comprise three distinct carbonate depositional facies [28].

Organic matter in the Marcellus Formation is dominated by originally hydrogen-rich unstructured (amorphous) bituminite and unicellular alginite [29–32]. Minor amounts of mostly oxidized and recycled humic material occur in most of the samples directly studied for this investigation. In the wet gas-producing region, the originally amorphous organic matter is severely degraded and converted to approximately equal amounts of solid hydrocarbon and pyrobitumen (Figure 3). VR_o in the wet gas region explicitly measured during this investigation is between 1.59 and 1.78%. Pyrobitumen dominates the organic matter in the dry gas-producing region where VR_o specifically measured during this study is between 2.35 and 4.61% (Figure 4). Pyrobitumen in the highest maturity Marcellus rocks ($>3.0\%$ VR_o) is highly aromatic and has undergone partial graphitization [12,30]. The Marcellus Formation in the subsurface of northeastern Pennsylvania is metagenetic and characterized by prehnite–pumpellyite to incipient greenschist metamorphic facies [12,30].

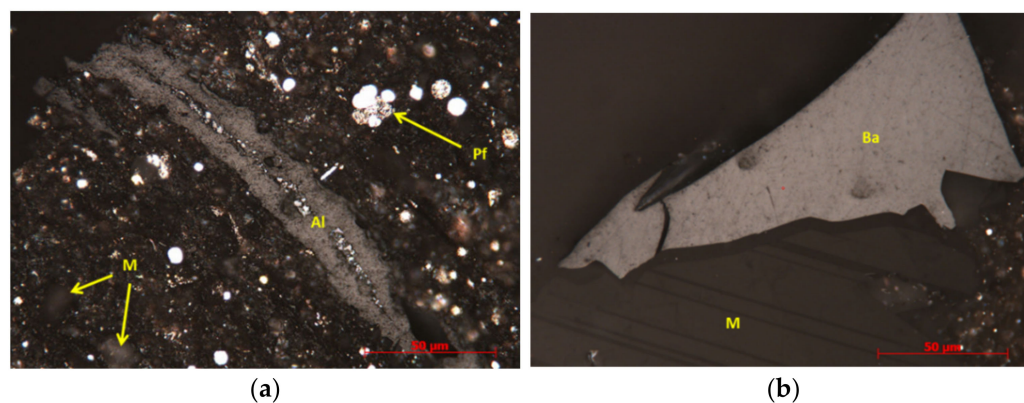


Figure 3. Photomicrographs of Marcellus Formation organic matter in Upshur County, West Virginia. Measured $VR_o = 2.37\%$. (a) Thermally transformed amorphous organic matter (AOM) with background matrix, mineral grains (M), framboidal pyrite (Pf) and interpreted algal body (Al). (b): Angular pyrobitumen (Ba) and interface with mineral matrix. Inert AOM comprises 46.1 to 57.9% of the kerogen. Solid hydrocarbon makes up between 25 and 40% of the organic matter. Conversion of AOM to hydrocarbon is estimated between 84.2 and 92.7%. Photomicrographs, composition interpretation, and VR_o measurements by Dr. Wayne Knowles, Stratum Laboratories, UK.

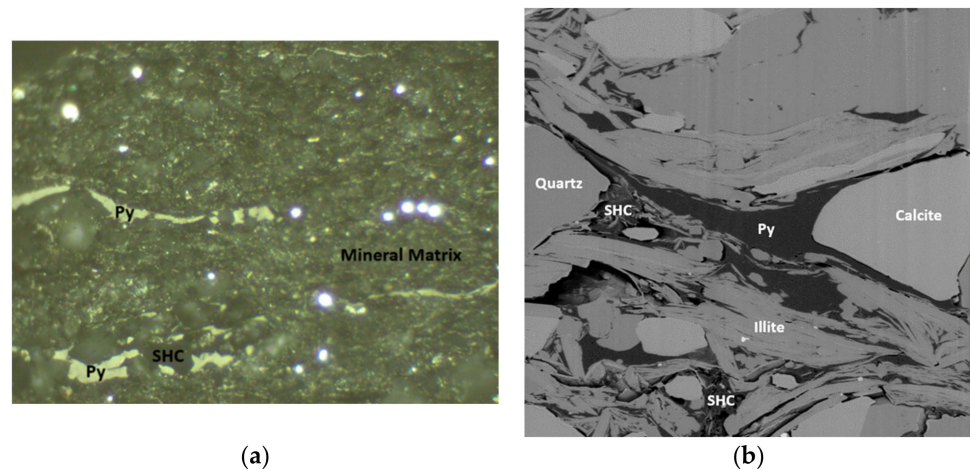


Figure 4. (a) Whole rock photomicrograph of pyrobitumen (Py) lenses and angular fragments, solid hydrocarbon (SHC), and mineral matrix in overmature ($VR_o = 4.56\%$) Marcellus Formation recovered in the Bennett #1 well, Sullivan County, Pennsylvania. (b) Backscatter electron (BE) SEM photomicrograph of the same sample. From Laughrey et al. [12].

Porosity in Marcellus Formation reservoirs is a function of compaction, cementation, and organic matter thermal maturation through the occlusion of primary void space and the development of secondary porosity [12,29,30]. Organic matter-hosted porosity provides the most significant portion of effective porosity and free-gas storage capacity in the reservoirs [12,29] (Figure 5). Matrix porosity is also present within the clay mineral aggregates and at the interface between rigid clasts and clay minerals [12,29].

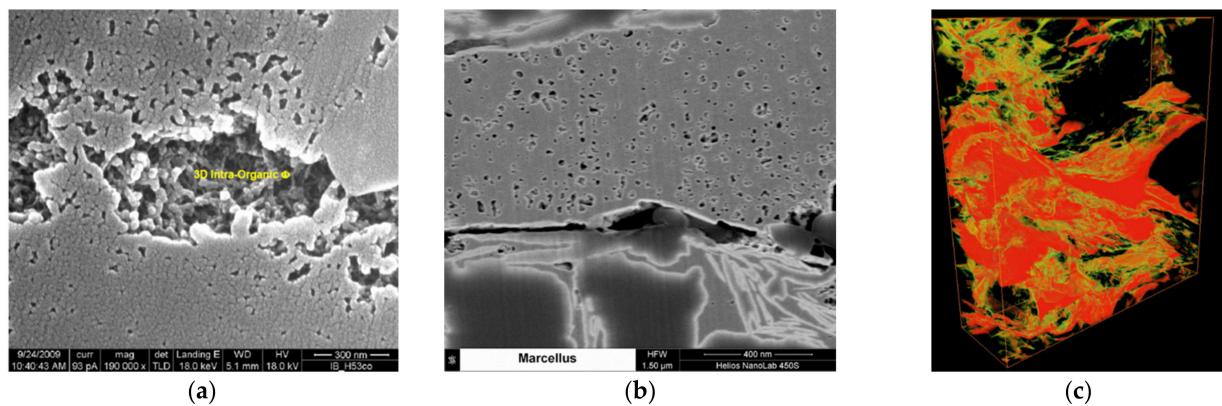


Figure 5. (a) Well-developed kerogen-hosted porosity, wet gas region southwestern Pennsylvania (SEM image courtesy William Zagorski, Range Resources). (b) Pyrobitumen-hosted organic porosity, dry gas region, northeastern Pennsylvania (from Laughrey et al. [12]). SEM images in (a) and (b) are the same scale. (c) 3D focused ion beam SEM model of interconnected pyrobitumen-hosted organic porosity in the same sample shown in (b). Red—pyrobitumen. Yellow—interconnected porosity. Horizontal field width = 8 μm .

Modeled maximum burial of Marcellus Formation strata in the wet gas-producing region was between 3.4 and 4 km (11,220 and 13,400 ft.) followed by uplift and erosion of 1.04 to 2.4 km (3419.6 to 8049.8 ft.) of Carboniferous and Permian overburden which was removed during post-Alleghenian uplift [33,34]. Modeled maximum burial in the dry gas-producing region was between 4.89 and 4.95 km (16,050 and 16,250 ft.) with subsequent uplift and erosion of 2.6 to 2.9 km (8550 to 9650 ft.) of overburden [33,34]. Higley and Enomoto [33] assigned the following rates of erosion of overburden sediments based on modeled thicknesses of erosion of nine wells in the study area: (A) 8.78 to 11.3 m/m.y. (28.8 to 37.1 ft./m.y.) from 260 Ma to Present; (B) 12.8 to 21.3 m/m.y. (42 to 70 ft./m.y.)

from 140 to 90 Ma; and (C) 50.3 to 83.8 m/m.y. (165 to 275 ft./m.y.) from 23.5 to 5.3 Ma. The latter two rates (B and C) represent two time periods of increased uplift and erosion.

3. Materials and Methods

Sixty-seven production gases were collected at the wellhead or separator in pressurized stainless-steel cylinders or Isotubes[®] and shipped to Isotech Laboratories in Champaign, IL, USA for processing and analyses (Tables 1 and 2). Thirty-four of these produced gas samples were collected in the dry gas region of northeast Pennsylvania (Bradford, Sullivan, Susquehanna, and Wyoming Counties). Two additional dry gas samples were collected in Upshur County, West Virginia. Twelve additional dry gas samples were collected from Marcellus Formation pressure core recovered from a well in Susquehanna County, Pennsylvania (Table 3). These 12 gas samples were collected during direct gas-in-place resource assessment in the laboratory. Thirty-one wet gas samples were collected in northwest and northcentral West Virginia (Tyler, Richie, Wetzel, Doddridge, and Harrison Counties) and southwest Pennsylvania (Washington County).

All gas samples were analyzed for chemical composition using a Shimadzu 2010 gas chromatograph. Quantification of fixed gases was done by thermal conductivity detector. Compositional data were processed on GC Solutions software and PC. Isotopic analyses were performed using traditional offline sample preparation techniques followed by dual inlet mass spectrometric ¹³C/¹²C measurement on a Finnigan MAT Delta S Isotope Ratio mass spectrometer. ²H/¹H measurements were performed on a Finnigan Delta Plus XL isotope ratio mass spectrometer. Sample results were compared with accepted reference standards (NGS #1, #2, or #3); isotope ratio determinations involved multiple direct comparisons of the sample to the reference standard (generally at least 6 comparisons). Stable carbon and hydrogen isotope compositions are reported as the difference between the ratios of the two isotopes of interest in the sample and the ratio in a primary reference standard. That is,

$$X_{\text{sample}} = [(R_{\text{sample}} - R_{\text{standard}})/R_{\text{standard}}] \times 1000, \quad (1)$$

where X represents the isotope of interest, in this case ¹³C and ²H or deuterium (D), and R represents the ratio of ¹³C/¹²C or ²H/¹H. The value is expressed in terms of per mil (‰), or parts per thousand.

Noble gas measurements were made on second splits of selected produced dry gas samples collected in stainless-steel pressurized cylinders at the same time as the gas samples analyzed at Isotech Laboratories (Tables 4 and 5). Noble gas measurements were performed using a ThermoFisher Helix Split Flight Type noble gas mass spectrometer at Smart Gas Sciences laboratories in Columbus, OH, USA.

Table 1. Marcellus Formation produced gas samples, chemical composition, and isotope ratios. nd—not detected. nm—not measured. * Concentration too small to measure isotope compositions. Sample data in bold blue print are time-lapse data discussed in the text. DG—dry gas. WG—wet gas. WV—West Virginia. PA—Pennsylvania.

| Well ID/Group | O ₂ Mole% | CO ₂ Mole% | N ₂ Mole% | C ₁ Mole% | C ₂ Mole% | C ₃ Mole% | iC ₄ Mole% | nC ₄ Mole% | iC ₅ mole% | nC ₅ Mole% | C ₆₊ Mole% | δ ¹³ C ₁ ‰ | δD _{C1} ‰ | δ ¹³ C ₂ ‰ | δ ¹³ C ₃ ‰ |
|---------------|----------------------|-----------------------|----------------------|----------------------|----------------------|----------------------|-----------------------|-----------------------|-----------------------|-----------------------|-----------------------|----------------------------------|--------------------|----------------------------------|----------------------------------|
| DG1 | 0.099 | 0.02 | 0.47 | 97.45 | 1.87 | 0.0755 | 0.0017 | 0.0047 | 0.0013 | 0.0008 | 0.0076 | −27.08 | −158.5 | −33.2 | −36.3 |
| DG2 | 0.086 | 0.039 | 0.42 | 97.38 | 1.97 | 0.0865 | 0.0033 | 0.0065 | 0.0027 | 0.0014 | 0.009 | −28.69 | −157.7 | −34.74 | −36.79 |
| DG3 | 0.13 | 0.019 | 0.5 | 97.5 | 1.79 | 0.0561 | 0.0007 | 0.0024 | nd | nd | 0.0018 | −27.85 | −158.2 | −34.1 | −36.8 |
| DG4 | 0.16 | 0.018 | 0.57 | 97.35 | 1.84 | 0.0594 | 0.0008 | 0.0027 | nd | nd | 0.001 | −27.85 | −159.3 | −34.13 | −36.9 |
| DG5 | 0.071 | 0.018 | 0.4 | 97.54 | 1.9 | 0.0659 | 0.001 | 0.0033 | 0.0001 | 0.0001 | 0.0004 | −27.95 | −158.2 | −34.22 | −36.9 |
| DG6 | 0.13 | 0.023 | 0.53 | 97.39 | 1.86 | 0.063 | 0.0009 | 0.0028 | nd | nd | nd | −28.5 | −157.8 | −34.96 | −37.4 |
| DG7 | 0.06 | 0.021 | 0.47 | 97.79 | 1.61 | 0.0486 | 0.0006 | 0.0022 | nd | nd | nd | −26.09 | −159.1 | −32.52 | −35.1 |
| DG8 | 0.015 | 0.023 | 0.4 | 97.82 | 1.69 | 0.0491 | 0.0006 | 0.0017 | nd | nd | nd | −25.96 | −159.9 | −32.48 | −35 |
| DG9 | 0.16 | 0.017 | 0.73 | 97.32 | 1.71 | 0.0607 | 0.0009 | 0.0032 | 0.0001 | 0.0001 | nd | −25.41 | −158.4 | −32.19 | −34.9 |
| DG10 | 0.037 | 0.016 | 0.57 | 97.62 | 1.69 | 0.0639 | 0.001 | 0.0033 | 0.0001 | 0.0001 | nd | −24 | −158.6 | −30.8 | −33.9 |
| DG11 | 0.36 | 0.022 | 2.04 | 96.12 | 1.41 | 0.0425 | 0.0006 | 0.0017 | 0.0001 | 0.0001 | 0.0004 | −24.04 | −163.9 | −29.9 | −32.5 |
| DG12 | nd | 0.061 | 0.57 | 97.87 | 1.42 | 0.032 | 0.0004 | 0.0008 | nd | nd | nd | −23.9 | nm | −29.86 | −31.4 |
| DG13 | 0.025 | 0.009 | 0.48 | 97.69 | 1.74 | 0.0571 | 0.0008 | 0.0025 | 0.0001 | 0.0001 | nd | −25.27 | −161.5 | −31.58 | −34.8 |
| DG14 | 0.094 | 0.019 | 0.6 | 97.6 | 1.63 | 0.0513 | 0.0007 | 0.0022 | nd | nd | nd | −25.03 | −160.3 | −31.28 | −34.2 |
| DG15 | 0.16 | 0.031 | 0.68 | 97.37 | 1.7 | 0.0565 | 0.0008 | 0.0025 | nd | nd | nd | −25.36 | −161.1 | −31.72 | −35 |
| DG16 | 0.19 | 0.033 | 0.7 | 96.74 | 2.22 | 0.108 | 0.0021 | 0.0067 | 0.0003 | 0.0002 | nd | −26.23 | −158.3 | −32.79 | −35.2 |
| DG17 | nd | 0.011 | 0.39 | 97.52 | 1.93 | 0.035 | 0.0003 | 0.0011 | nd | nd | nd | −36.2 | nm | −42.11 | −43 |
| DG18 | nd | 0.017 | 0.38 | 97.05 | 2.41 | 0.093 | 0.0016 | 0.0058 | 0.0002 | 0.0002 | nd | −31.41 | nm | −38.73 | −40.9 |
| DG19 | 0.043 | 0.065 | 27.06 | 55.27 | 0.02 | nd | nd | 0.0001 | nd | nd | 0.0009 | −59.58 | nm | −32.7 | * |
| DG20 | nd | 0.028 | 0.23 | 97.57 | 2.09 | 0.057 | 0.0007 | 0.002 | nd | nd | nd | −29.34 | nm | −35.46 | −37.8 |
| DG21 | 0.06 | 0.021 | 0.4 | 97.02 | 2.37 | 0.0868 | 0.0014 | 0.0047 | 0.0002 | 0.0001 | nd | −30.8 | nm | −37.74 | −39.9 |
| DG22 | 0.016 | 0.042 | 0.28 | 97.33 | 2.21 | 0.0716 | 0.001 | 0.0033 | 0.0001 | 0.0001 | nd | −35.91 | nm | −41.13 | −43 |
| DG23 | 0.027 | 0.01 | 0.38 | 96.4 | 2.63 | 0.101 | 0.0016 | 0.0054 | 0.0002 | 0.0001 | nd | −33.57 | nm | −39.94 | −42.1 |
| DG24 | 0.056 | 0.029 | 0.42 | 96.99 | 2.37 | 0.0948 | 0.0016 | 0.0055 | 0.0002 | 0.0002 | nd | −28.78 | nm | −35.95 | −37.5 |
| DG25 | 0.11 | 0.037 | 0.61 | 96.78 | 2.33 | 0.0926 | 0.0015 | 0.004 | 0.0001 | 0.0001 | nd | −26.44 | nm | −33.4 | −34.6 |
| DG26 | 0.015 | nd | 0.37 | 94.45 | 2.48 | 0.105 | 0.0018 | 0.0062 | 0.0003 | 0.0002 | nd | −28.36 | nm | −34.97 | −37.6 |
| DG27 | 0.039 | 0.012 | 0.37 | 96.94 | 2 | 0.0505 | 0.001 | 0.0067 | 0.0004 | 0.0003 | nd | −31.12 | nm | −38.13 | −40.8 |
| DG28 | 0.038 | 0.009 | 0.69 | 96.46 | 2.31 | 0.0812 | 0.0013 | 0.0045 | 0.0002 | 0.0001 | 0.0049 | −33.98 | nm | −40.16 | −42.3 |
| DG29 | 0.2 | 0.014 | 1.02 | 96.44 | 2.11 | 0.0639 | 0.0009 | 0.0023 | nd | nd | nd | −27.29 | nm | −33.52 | −35.9 |
| DG30 | 0.055 | 0.031 | 0.55 | 97.56 | 1.71 | 0.0454 | 0.0005 | 0.0014 | nd | nd | nd | −24.94 | nm | −31.16 | −33.3 |
| DG31 | 0.045 | 0.026 | 0.49 | 97.62 | 1.74 | 0.0447 | 0.0005 | 0.0014 | nd | nd | nd | −25.13 | nm | −31.44 | −33.6 |
| DG32 | 0.048 | 0.03 | 0.62 | 97.81 | 1.39 | 0.0336 | 0.0004 | 0.0011 | nd | nd | nd | −23.53 | nm | −29.86 | −32 |
| DG33 | 0.052 | 0 | 0.74 | 96.78 | 0.546 | 0.0048 | nd | nd | nd | nd | nd | −23.59 | nm | −29.59 | * |
| DG34 | 0.034 | 0.015 | 0.96 | 97.42 | 1.44 | 0.0385 | 0.0005 | 0.0012 | nd | nd | 0.0054 | −24.63 | nm | −30.89 | −33.1 |
| WVDG1 | nd | nd | nd | 95.8 | 2.26 | 0.1329 | 0.0003 | 0.0064 | 1.82 | 0.013 | 0.003 | −39.1 | nm | −41.7 | −38.9 |
| WVDG2 | nd | nd | nd | 97 | 1.845 | 0.0579 | 0.0003 | 0.0034 | 1.074 | 0.0045 | 0.0069 | −39.2 | nm | −41.9 | −40.7 |
| WG1 | 0.016 | 0.15 | 0.4 | 80.85 | 12.95 | 3.68 | 0.471 | 0.817 | 0.22 | 0.187 | 0.236 | −43.7 | −189.2 | −32.74 | −28 |
| WG2 | nd | 0.17 | 0.51 | 75.4 | 15.61 | 5.49 | 0.573 | 1.4 | 0.272 | 0.317 | 0.223 | −45.5 | −200.8 | −35.28 | −30.34 |

Table 1. Cont.

| Well ID/Group | O ₂ Mole% | CO ₂ Mole% | N ₂ Mole% | C ₁ Mole% | C ₂ Mole% | C ₃ Mole% | iC ₄ Mole% | nC ₄ Mole% | iC ₅ mole% | nC ₅ Mole% | C ₆₊ Mole% | δ ¹³ C ₁ ‰ | δD _{C1} ‰ | δ ¹³ C ₂ ‰ | δ ¹³ C ₃ ‰ |
|---------------|----------------------|-----------------------|----------------------|----------------------|----------------------|----------------------|-----------------------|-----------------------|-----------------------|-----------------------|-----------------------|----------------------------------|--------------------|----------------------------------|----------------------------------|
| WG3 | 0.017 | 0.15 | 0.48 | 78.94 | 13.72 | 4.26 | 0.493 | 1.02 | 0.255 | 0.255 | 0.351 | −45.73 | −201.4 | −34.34 | −29.63 |
| WG4 | 0.015 | 0.14 | 0.48 | 76.41 | 14.88 | 5.2 | 0.614 | 1.37 | 0.299 | 0.319 | 0.243 | −45.41 | −201.5 | −34.41 | −29.7 |
| WG5 | 0.013 | 0.17 | 0.43 | 77.02 | 14.83 | 4.87 | 0.556 | 1.21 | 0.281 | 0.3 | 0.284 | −44.97 | −196.6 | −34.1 | −29.39 |
| WG6 | 0.011 | 0.18 | 0.47 | 79.62 | 13.36 | 4.1 | 0.528 | 0.964 | 0.255 | 0.225 | 0.247 | −44.94 | −191.1 | −33.67 | −29.04 |
| WG7 | 0.015 | 0.17 | 0.54 | 79.21 | 13.28 | 4.26 | 0.541 | 1.07 | 0.277 | 0.274 | 0.328 | −45.21 | −195.4 | −34.01 | −29.48 |
| WG8 | 0.011 | 0.16 | 0.44 | 78.77 | 13.87 | 4.32 | 0.508 | 1.05 | 0.255 | 0.259 | 0.31 | −45.25 | −197.5 | −33.98 | −29.13 |
| WG9 | 0.011 | 0.14 | 0.46 | 78.84 | 13.71 | 4.38 | 0.538 | 1.09 | 0.274 | 0.268 | 0.246 | −45.38 | −198.2 | −33.94 | −29.17 |
| WG10 | 0.015 | 0.16 | 0.44 | 78.77 | 13.85 | 4.31 | 0.506 | 1.05 | 0.258 | 0.267 | 0.328 | −45.22 | −198.4 | −33.9 | −29.08 |
| WG11 | 0.013 | 0.16 | 0.44 | 78.94 | 13.83 | 4.27 | 0.495 | 1.02 | 0.245 | 0.25 | 0.289 | −45.24 | −198.3 | −33.91 | −29.11 |
| WG12 | 0.012 | 0.14 | 0.5 | 76.61 | 14.69 | 5.12 | 0.618 | 1.35 | 0.317 | 0.326 | 0.288 | −45.5 | −203.1 | −34.63 | −29.87 |
| WG13 | 0.095 | 0.16 | 0.71 | 69.37 | 16.68 | 6.86 | 0.854 | 2.33 | 0.578 | 0.81 | 1.53 | −45.23 | −197.6 | −35.12 | −30.15 |
| WG14 | 0.012 | 0.15 | 0.5 | 71.89 | 16.14 | 6.14 | 0.847 | 1.84 | 0.381 | 0.469 | 0.83 | −45.19 | −200.9 | −35.14 | −30.2 |
| WG15 | 0.014 | 0.21 | 0.34 | 90.49 | 7.56 | 1.04 | 0.118 | 0.115 | 0.0288 | 0.0137 | 0.0235 | −42.25 | −174.4 | −31.2 | −25.67 |
| WG16 | 0.32 | 0.14 | 1.4 | 92.27 | 5.27 | 0.457 | 0.0333 | 0.0356 | 0.0058 | 0.0029 | 0.004 | −40.15 | −167.2 | −33.34 | −28.18 |
| WG17 | nd | 0.15 | 0.54 | 76.52 | 14.52 | 5.11 | 0.632 | 1.4 | 0.304 | 0.269 | 0.456 | −46.74 | −210.6 | −35.87 | −31.05 |
| WG18 | nd | 0.18 | 0.42 | 84.51 | 10.64 | 2.41 | 0.358 | 0.507 | 0.184 | 0.133 | 0.568 | −42.98 | −179.5 | −32.15 | −27.18 |
| WG19 | nd | 0.2 | 0.33 | 90.96 | 7.35 | 0.876 | 0.082 | 0.0897 | 0.0202 | 0.0108 | 0.0456 | −40.83 | −172.1 | −31.38 | −26.33 |
| WG20 | nd | 0.18 | 0.43 | 80.35 | 13.42 | 3.75 | 0.473 | 0.805 | 0.197 | 0.159 | 0.192 | −44.06 | −186.6 | −33.11 | −28.54 |
| WG21 | nd | 0.15 | 0.44 | 79.2 | 13.84 | 4.23 | 0.498 | 0.998 | 0.213 | 0.205 | 0.185 | −45.27 | −192.5 | −33.9 | −29.13 |
| WG22 | nd | 0.15 | 0.39 | 82.48 | 12.38 | 3.1 | 0.392 | 0.599 | 0.157 | 0.112 | 0.205 | −43.21 | −179.4 | −32.37 | −27.56 |
| WG23 | nd | 0.16 | 0.48 | 83.37 | 11.49 | 2.98 | 0.379 | 0.624 | 0.164 | 0.124 | 0.177 | −44.53 | −184.9 | −33.17 | −28.48 |
| WG24 | nd | 0.16 | 0.47 | 83.14 | 11.41 | 3.1 | 0.427 | 0.691 | 0.196 | 0.143 | 0.204 | −44.61 | −186.7 | −33.28 | −28.75 |
| WG25 | nd | 0.15 | 0.49 | 74.93 | 16.48 | 5.58 | 0.549 | 1.25 | 0.198 | 0.221 | 0.125 | −44.97 | −200.4 | −34.66 | −29.78 |
| WG26 | 0.014 | 0.15 | 0.52 | 81.85 | 12.29 | 3.32 | 0.359 | 0.598 | 0.164 | 0.175 | 0.502 | −45.29 | −196 | −33.89 | −29.18 |
| WG27 | nd | 0.12 | 0.39 | 73.07 | 15.61 | 6.01 | 0.868 | 1.73 | 0.369 | 0.409 | 0.813 | −44.5 | −242.8 | −33.82 | −29.25 |
| WV28 | 0.015 | 0.13 | 0.39 | 73.49 | 15.21 | 5.65 | 0.852 | 1.62 | 0.378 | 0.413 | 1.18 | −44.36 | −197.7 | −33.69 | −28.96 |
| PAWG1 | nd | 0.086 | 0.57 | 70.64 | 16.42 | 7.81 | 0.792 | 2.2 | 0.387 | 0.555 | 0.49 | −45.23 | −212.3 | −35.84 | −31.22 |
| PAWG2 | nd | 0.085 | 0.49 | 77.24 | 14.48 | 5.24 | 0.544 | 1.15 | 0.215 | 0.243 | 0.249 | −43.82 | −193.5 | −33.83 | −29.37 |
| PAWG3 | nd | 0.084 | 0.47 | 79.79 | 12.67 | 4.32 | 0.519 | 1.1 | 0.261 | 0.287 | 0.434 | −42.19 | −185.4 | −33.15 | −28.46 |

Table 2. Additional isotope ratios for selected samples. nm—not measured.

| Well ID/Group | $\delta^{13}\text{C}_2$ ‰ | $\delta^{13}\text{CO}_2$ ‰ | $\delta^{15}\text{N}_2$ ‰ |
|---------------|------------------------------|-------------------------------|------------------------------|
| DG1 | −188.2 | nm | nm |
| DG2 | −190.6 | nm | nm |
| DG3 | −191.6 | nm | nm |
| DG4 | −191.5 | nm | nm |
| DG5 | −192 | nm | nm |
| DG6 | −189.7 | nm | nm |
| DG7 | −188.9 | nm | nm |
| DG8 | −192.6 | nm | nm |
| DG9 | −191.3 | nm | nm |
| DG10 | −190.4 | nm | nm |
| DG11 | −189.4 | nm | −10.223 |
| DG12 | nm | −26.5 | nm |
| DG13 | −192.9 | nm | nm |
| DG14 | −189.4 | nm | nm |
| DG15 | −190.9 | nm | nm |
| DG16 | −190.9 | nm | nm |
| DG19 | nm | −31.8 | nm |
| PAWG1 | −171.4 | nm | −13.9 |
| PAWG2 | −162.7 | nm | −13.3 |
| PAWG3 | −162.4 | nm | −12.7 |

Table 3. Pressure core isotope ratio and cumulative degassing volume results. Nm—not measured.

| Cumulative Degassing Volume % | $\delta^{13}\text{C}_1$ ‰ | $\delta^{13}\text{C}_2$ ‰ | $\delta^{13}\text{C}_3$ ‰ |
|----------------------------------|------------------------------|------------------------------|------------------------------|
| 21.77 | −26.3 | −31 | nm |
| 22.93 | −26.88 | −32.7 | −34.8 |
| 33.12 | −27.64 | −33.15 | −33.5 |
| 25.47 | −27.31 | −32.93 | −35.1 |
| 28.45 | −27.49 | −32.92 | −32.3 |
| 37.52 | −27.62 | −33.39 | −33.57 |
| 40.69 | −27.68 | −33.45 | −35 |
| 53.53 | −27.03 | −33.5 | −35 |
| 66.03 | −26.25 | −32.94 | −34.8 |
| 75.35 | −25.63 | −33.45 | −34.7 |
| 71.81 | −25.69 | −33.24 | −34.8 |
| 100 (crushed gas) | −22.8 | −29.1 | −34.7 |

Twenty-three condensate samples, co-produced with the wet gases described above, were collected as dead oil (i.e., collected at atmospheric pressure and lacking volatiles) at the separator in glass jars with Teflon lids and shipped to Stratum Reservoir Laboratories in Houston, Texas USA (Table 6). High-Resolution Gas Chromatography (HRGC) was performed using an Agilent 6890 GC-FID instrument. API gravity was derived from measurement of specific gravity by hydrometer (ASTM D1298).

Excepting the pressure core gas samples, all of the fluid samples were collected from horizontal wells stimulated by hydraulic fracturing. The Marcellus reservoir samples represent the landing zones of the wells and are not necessarily from the exact petroleum source rock intervals of the produced gas and condensate.

Table 4. Noble gas concentrations and isotope ratios of selected Marcellus Formation dry gas samples. Concentration prefixes are p = pico (10^{-12}), n = nano (10^{-9}), μ = micro (10^{-6}). R/R_a is the ratio of helium isotopes in the sample divided by the ratio in air = $(^3\text{He}/^4\text{He})_{\text{measured}}/(^3\text{He}/^4\text{He})_{\text{air}}$. Selected characteristic noble gas ratios for water and crust are included for comparison. Note that the water ratios are determined from the relative solubility of atmospheric noble gases in contact with water. The ^{84}Kr and ^{132}Xe are fission products of uranium and their concentrations are dependent upon the uranium content of the crustal rocks. ^{21}Ne is generated by the α particle produced by uranium decay reacting with oxygen and magnesium in the rock. ^{40}Ar is produced by the radioactive decay of K.

| Well | ^3He pcc/cc | ^4He $\mu\text{cc}/\text{cc}$ | ^{20}Ne $\mu\text{cc}/\text{cc}$ | ^{21}Ne $\mu\text{cc}/\text{cc}$ | ^{22}Ne $\mu\text{cc}/\text{cc}$ | Ne $\mu\text{cc}/\text{cc}$ | ^{36}Ar $\mu\text{cc}/\text{cc}$ | ^{38}Ar $\mu\text{cc}/\text{cc}$ | ^{40}Ar $\mu\text{cc}/\text{cc}$ | Ar $\mu\text{cc}/\text{cc}$ | ^{84}Kr ncc/cc | Kr ncc/cc | ^{132}Xe ncc/cc | Xe ncc/cc |
|------|-------------------------|---|--|--|--|---|--|--|--|---|---|---|---|---|
| DG19 | 39.67 | 501.6 | 6.53 | 2.609 | 93.25 | 9.14 | 9.65 | 1.97 | 3088.4 | 3100.0 | 132.14 | 231.9 | 3.720 | 13.8 |
| DG17 | 4.56 | 298.2 | 0.45 | 0.002 | 0.06 | 0.46 | 0.29 | 0.06 | 108.6 | 109.0 | 6.63 | 11.6 | 0.164 | 0.6 |
| DG12 | 41.17 | 774.3 | 0.07 | 0.001 | 0.05 | 0.07 | 0.22 | 0.04 | 90.9 | 91.1 | 6.33 | 11.1 | 0.335 | 1.2 |
| DG20 | 27.42 | 276.2 | 1.46 | 0.005 | 0.18 | 1.46 | 0.67 | 0.13 | 216.7 | 217.5 | 64.00 | 112.3 | 4.713 | 17.5 |
| DG18 | 17.23 | 300.1 | 0.23 | 0.001 | 0.03 | 0.23 | 0.30 | 0.06 | 93.9 | 94.2 | 9.46 | 16.6 | 0.377 | 1.4 |
| Well | R/Ra | $\frac{^{20}\text{Ne}}{^{22}\text{Ne}}$ | $\frac{^{21}\text{Ne}}{^{22}\text{Ne}}$ | $\frac{^{38}\text{Ar}}{^{36}\text{Ar}}$ | $\frac{^{40}\text{Ar}}{^{36}\text{Ar}}$ | $\frac{^{82}\text{Kr}}{^{84}\text{Kr}}$ | $\frac{^{83}\text{Kr}}{^{84}\text{Kr}}$ | $\frac{^{86}\text{Kr}}{^{84}\text{Kr}}$ | $\frac{^{128}\text{Xe}}{^{132}\text{Xe}}$ | $\frac{^{129}\text{Xe}}{^{132}\text{Xe}}$ | $\frac{^{130}\text{Xe}}{^{132}\text{Xe}}$ | $\frac{^{131}\text{Xe}}{^{132}\text{Xe}}$ | $\frac{^{134}\text{Xe}}{^{132}\text{Xe}}$ | $\frac{^{136}\text{Xe}}{^{132}\text{Xe}}$ |
| DG19 | 0.057 | 9.597 | 0.0289 | 0.204 | 320.100 | 0.194 | 0.248 | 0.297 | 0.146 | 0.973 | 0.148 | 0.828 | 0.394 | 0.354 |
| DG17 | 0.011 | 8.223 | 0.0332 | 0.189 | 373.200 | 0.190 | 0.247 | 0.294 | 0.135 | 0.985 | 0.155 | 0.802 | 0.452 | 0.422 |
| DG12 | 0.038 | 9.674 | 0.0311 | 0.189 | 404.100 | 0.194 | 0.242 | 0.289 | 0.181 | 0.992 | 0.160 | 0.821 | 0.411 | 0.348 |
| DG20 | 0.071 | 9.472 | 0.0290 | 0.200 | 324.600 | 0.190 | 0.252 | 0.295 | 0.114 | 0.965 | 0.134 | 0.800 | 0.396 | 0.365 |
| DG18 | 0.041 | 9.597 | 0.0341 | 0.198 | 315.690 | 0.176 | 0.224 | 0.277 | 0.157 | 0.965 | 0.136 | 0.799 | 0.398 | 0.346 |

Table 5. Select sample noble gas ratios compared to water and crustal ratios.

| | R/Ra | $\frac{^{20}\text{Ne}}{^{22}\text{Ne}}$ | $\frac{^{21}\text{Ne}}{^{22}\text{Ne}}$ | $\frac{^{40}\text{Ar}}{^{36}\text{Ar}}$ | $\frac{^{84}\text{Kr}}{^{36}\text{Ar}}$ | $\frac{^{132}\text{Xe}}{^{84}\text{Kr}}$ | $\frac{^4\text{He}}{^{40}\text{Ar}^*}$ | $\frac{^{21}\text{Ne}^*}{^{40}\text{Ar}^*}$ | $\frac{^{20}\text{Ne}}{^{36}\text{Ar}}$ | $\frac{^{84}\text{Kr}}{^{36}\text{Ar}}$ |
|--------------|-------|---|---|---|---|--|--|---|---|---|
| Water | 1 | 9.8 | 0.029 | 295.5 | 0.038 | 0.021 | | | | |
| Crust | 0.02 | 0.09 | 0.450 | 3000 | 0.029 | 0.138 | | | | |
| DG19 | 0.057 | 9.597 | 0.0289 | 320.100 | 0.0137 | 0.028 | 196.7 | 0 | 0.677 | 0.014 |
| Dg17 | 0.011 | 8.223 | 0.0332 | 373.200 | 0.0228 | 0.025 | 1.12 | 0.43 | 1.559 | 0.023 |
| DG12 | 0.038 | 9.674 | 0.0311 | 404.100 | 0.0281 | 0.053 | 1.60 | 0 | 0.294 | 0.028 |
| DG20 | 0.071 | 9.472 | 0.0290 | 324.600 | 0.0959 | 0.074 | 6.343 | 0 | 2.180 | 0.096 |
| DG18 | 0.041 | 9.597 | 0.0341 | 315.690 | 0.0318 | 0.040 | 4.42 | 43.3 | 0.765 | 0.032 |

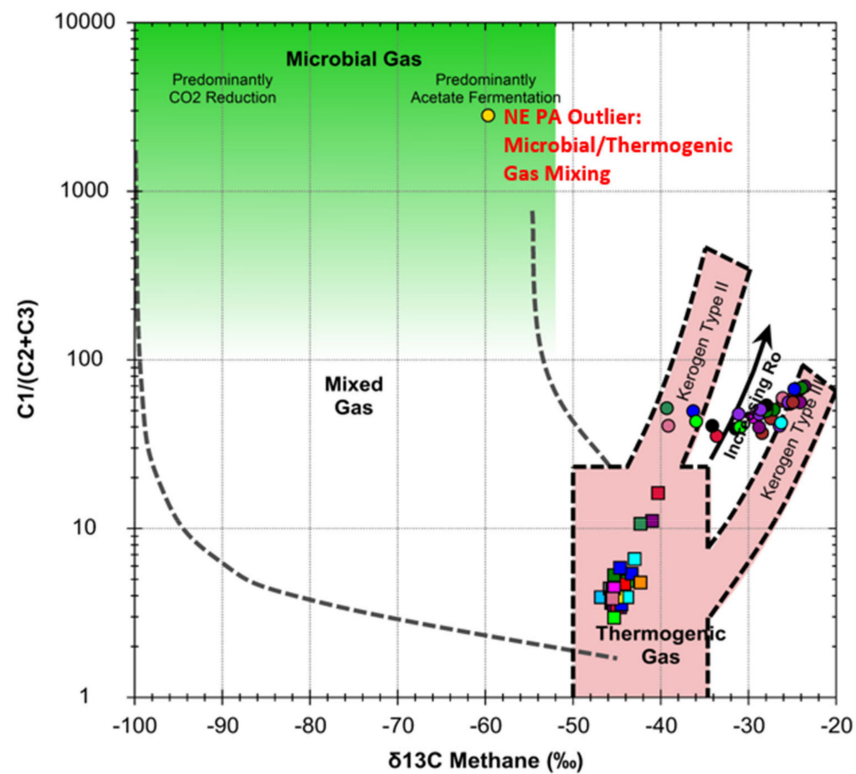
Table 6. Condensate data for selected wells.

| Well ID/Group | °API Gravity | C ₇ Temp °C | Pristane/Phytane | Toluene/nC ₇ | nC ₇ /MCH | Heptane Ratio | Isoheptane Ratio |
|---------------|--------------|------------------------|------------------|-------------------------|----------------------|---------------|------------------|
| WG1 | 65.5 | 129.27 | 1.84 | 0.17 | 1.37 | 31.3 | 9.16 |
| WG2 | 74.6 | 131.88 | 1.94 | 0.11 | 1.83 | 33.56 | 8.55 |
| WG3 | 69.8 | 131.09 | 1.48 | 0.16 | 1.63 | 32.93 | 9.18 |
| WG4 | 69.6 | 131.47 | 2.05 | 0.14 | 1.87 | 34.05 | 9.98 |
| WG5 | 69.4 | 130.17 | 1.42 | 0.13 | 1.74 | 33.95 | 9.92 |
| WG6 | 70.9 | 131.23 | 1.35 | 0.21 | 1.12 | 29.85 | 5.71 |
| WG7 | 57.8 | 132.03 | 1.35 | 0.2 | 1.16 | 30.72 | 5.09 |
| WG8 | 65.3 | 130.05 | 1.58 | 0.15 | 1.64 | 33.91 | 9.75 |
| WG9 | 68.3 | 130.86 | 1.7 | 0.16 | 1.67 | 32.99 | 10.05 |
| WG10 | 66.5 | 130.04 | 1.62 | 0.15 | 1.67 | 33.91 | 9.93 |
| WG11 | 64.8 | 129.79 | 1.61 | 0.16 | 1.65 | 34.07 | 9.86 |
| WG12 | 73 | 132.21 | 1.94 | 0.14 | 1.81 | 33.36 | 9.26 |
| WG13 | - | 131.2 | 1.91 | 0.11 | 1.88 | 34.29 | 8.94 |
| WG14 | 70.8 | 130.7 | 1.92 | 0.106 | 1.95 | 34.8 | 9.25 |
| WG18 | 60.1 | 129.23 | 1.88 | 0.2 | 1.17 | 30.45 | 7.34 |
| WG20 | 57.4 | 130.1 | 1.38 | 0.22 | 1.14 | 30.16 | 6.34 |
| WG21 | 70.4 | 130.9 | 2.21 | 0.14 | 1.76 | 33.36 | 10.43 |
| WG23 | - | 130.5 | 1.61 | 0.232 | 1.21 | 28.86 | 8.58 |
| WG24 | 58.4 | 131.55 | 1.43 | 0.2 | 1.12 | 27.33 | 8.15 |
| WG25 | 53.2 | 131.1 | 1.89 | 0.12 | 1.97 | 34.45 | 9.77 |
| WG26 | - | 131.6 | 1.38 | 0.41 | 1.16 | 30.9 | 5.41 |
| WG27 | - | 131.5 | 2 | 0.12 | 1.78 | 33.92 | 9.46 |
| WV28 | - | 131.7 | 1.82 | 0.17 | 1.71 | 32.32 | 9.97 |
| PAWG1 | 74.6 | - | - | - | - | - | - |
| PAWG2 | 53.2 | - | - | - | - | - | - |

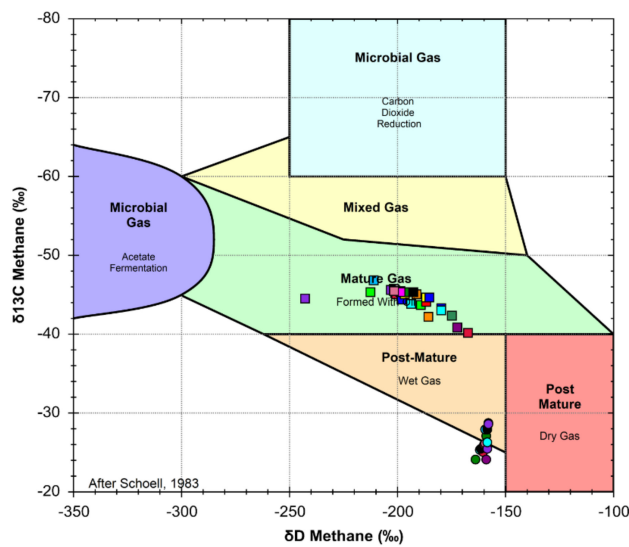
4. Results and Discussion

4.1. Bulk Composition and Stable Isotopes of Produced Gases

Samples collected in the wet gas-producing region exhibit bulk compositions and isotope ratios characteristic of oil-associated thermogenic gases [35–38] (Figure 6). Methane (C_1) concentrations range from 69.37 to 92.27 mole%, with $\delta^{13}C_1$ ranging from -46.74 to -40.15 ‰ VPDB and δD_{CH_4} from -243.8 to -167.2 ‰ VSMOW. Ethane (C_2) and propane (C_3) concentrations are between 5.27 and 16.68 and 0.5 and 7.81 mole%, respectively.



(a)



(b)

Figure 6. (a): Methane $\delta^{13}C$ versus $C_1/(C_2/C_3)$ for wet (squares) and dry (circles) Marcellus Formation produced gases in the Appalachian basin (after Bernard et al. [35]). The different colors represent the various gas samples listed in Table 1 (b) Schoell [36] plot of methane δD versus $\delta^{13}C$ for the Marcellus produced gases in the Appalachian basin.

All but one of the production gas samples collected in the dry gas-producing region exhibit bulk compositions typical of high-maturity thermogenic gas [35–38] (Figure 6). The gases are composed primarily of methane, with small volumes of ethane and trace contributions of propane and butane+ (C_{4+}). Methane concentrations range from 94.45 to 97.87 mole%. One anomalous sample contains only 55.27 mole% C_1 due to a high nitrogen (N_2) content related to air contamination as confirmed by a N_2/Ar ratio similar to that of air. Isotope ratios of hydrocarbon gases are consistent with a thermogenic origin, with $\delta^{13}C_1$ ranging from -39.2 to -23.53% VPDB and δD_{CH_4} from -163.9 to -157.7% VSMOW (Figure 6b). Both ranges indicate a thermogenic origin of methane without any contribution from a microbial source [33–36] (Figure 6). The one produced gas sample with only 55.25 mole% C_1 is an exception: it has a $\delta^{13}C_{CH_4}$ of -59.58% VPDB and a $C_1/(C_2 + C_3)$ ratio of 2763.5 indicating mixing with microbial methane [32,33] (Figure 6a).

The Marcellus Formation gases from both the dry gas-producing region and the wet gas-producing region show a general trend of enrichment in ^{13}C as the gases become richer in methane (Figure 6a). However, there is considerable scatter in $^{13}C_1$ of the dry gas samples compared to the wet gas samples due to the shifting fields for kerogen type on the plot of $^{13}C_1$ against $C_1/(C_2 + C_3)$. The shift from kerogen type II to kerogen type III exhibited by the dry gas samples in Figure 6a is a function of increasing thermal maturity accompanied by decreasing atomic H/C in the parent organic matter, and not due to variation in organic facies. Hydrogen Index (HI) and Oxygen Index (OI) decrease across the basin from average respective values of 529–582 mg hydrocarbon/g TOC and 15–34 mg CO_2 /g TOC in thermally immature to mature Marcellus samples [31,32] to 6–31 mg hydrocarbon/g TOC and 7–9 mg CO_2 /g TOC in overmature Marcellus samples [12]. Respective H/C and O/C ratios in the latter are as low as 0.40 and 0.06 [12].

The respective $\delta^{13}C$ values of ethane and propane in the wet gas samples range between -35.87 and -31.2% and -31.22 and -25.67% (Figure 7a). The wet gases exhibit normal kinetic isotope trends on the natural gas plot shown in Figure 7a, with $\delta^{13}C_1 < \delta^{13}C_2 < \delta^{13}C_3$. Deviations from a straight line in Figure 7a indicate a mixture of source inputs, heterogeneity in the organic source material, and/or secondary hydrocarbon gas alteration effects [39,40]. By contrast, the ethane $\delta^{13}C$ of dry gas samples ranges from -42.11 to -29.59% and the propane $\delta^{13}C$ of the dry gases ranges from -43 to -31.4% (Figure 7b). All the samples collected from the dry gas-producing region exhibit full carbon isotope reversals with $\delta^{13}C_1 > \delta^{13}C_2 > \delta^{13}C_3$ (Figure 7b). The δD ratios of the dry gas samples are reversed as well with $\delta D_{CH_4} > \delta D_{C_2}$ (Figure 8). Wet gases, by comparison, exhibit normal hydrogen isotope trends with $\delta D_{CH_4} < \delta D_{C_2}$ (Figure 8). The carbon and hydrogen isotope reversals observed in the dry gas samples are considered in detail in Section 4.6 below.

Figure 9 is a plot of gas wetness versus $\delta^{13}C_2$ for all the samples from both the wet and dry gas-producing regions. Beginning at measured $VR_o = 1.59\%$, the wet gases plot along the expected thermal maturity trend defined by decreasing wetness and increasing $\delta^{13}C_2$. However, the most thermally mature wet gas sample does not follow the expected maturity trend. It “rolls over”, i.e., exhibits decreasing wetness accompanied by decreasing $\delta^{13}C_2$. Rollover occurs at a wetness of about 5.9% and $VR_o = 1.78\%$. Dry gases with full isotopic reversals (Figures 7 and 8) exhibit rapidly decreasing wetness (~ 4 to 1.4%) and sharply increasing $\delta^{13}C_2$ between measured VR_o values of 2.35 and 4.61%.

Non-hydrocarbon gases produced from the Marcellus reservoirs are present in much smaller amounts, with CO_2 concentrations up to 0.21 mole% in the wet gas-producing region and 0.061 mole% in the dry gas-producing region. $\delta^{13}CO_2$ was measured for two dry produced gas samples. $\delta^{13}CO_2 = -26.5\%$ in the DG12 gas and -31.8% in the DG19 gas (Table 2). These values indicate an organic, high maturity thermogenic origin for the CO_2 [37]. Excepting the one air-contaminated sample (DG19), N_2 concentrations in the dry gas region are between 0.4 and 2.04 mole%. $\delta^{15}N$ was measured in the DG12 sample and is -10.2% (Table 2). Nitrogen concentrations in the wet gas region are between 0.33 and 1.4 mole%. $\delta^{15}N$ measured in three of the wet gas samples is between -13.9 and -12.7% . These isotopically light $\delta^{15}N$ values indicate a thermogenic organic nitrogen source [37].

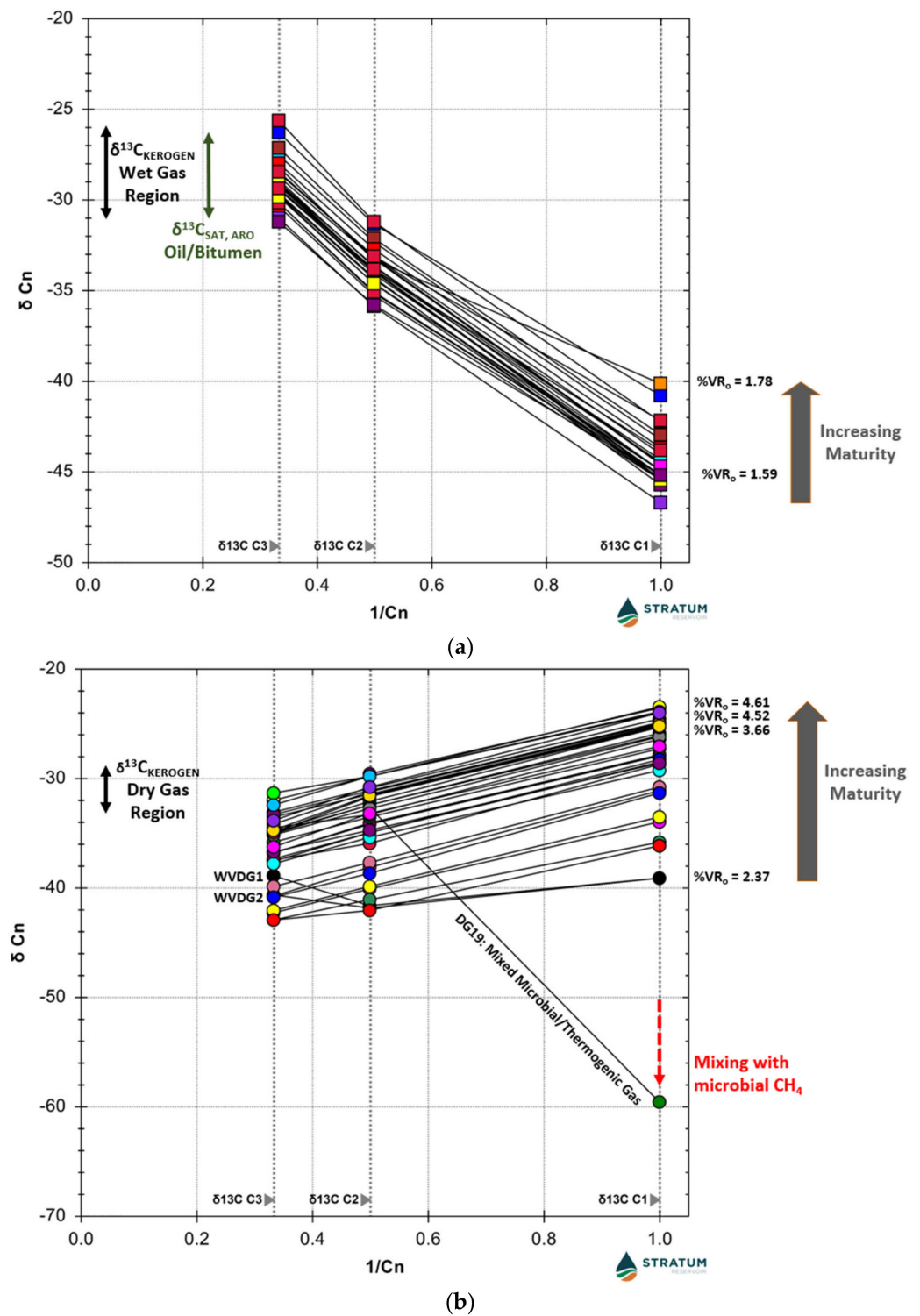


Figure 7. (a): Natural gas plot for wet Marcellus Formation produced gases (after Chung et al. [39]). Kerogen and oil/bitumen $\delta^{13}C$ range [12] is shifted right of the y-axis for clarity. (b) Natural gas plot for dry Marcellus Formation produced gases. VR_o measurements by Dr. Wayne Knowles, Stratum Laboratories.

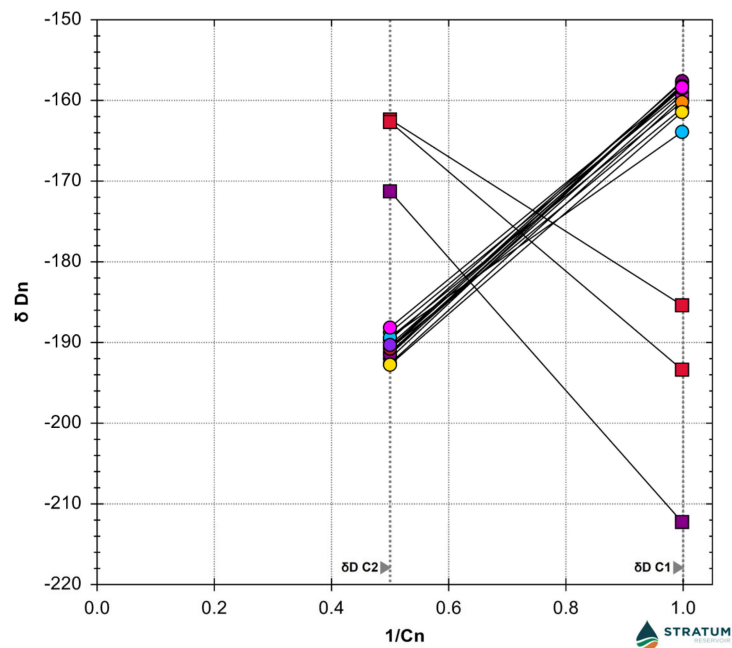


Figure 8. Natural gas plot of hydrogen isotope ratios for wet (squares) and dry (circles) Marcellus Formation produced natural gases in the Appalachian basin (after Chung et al. [39]).

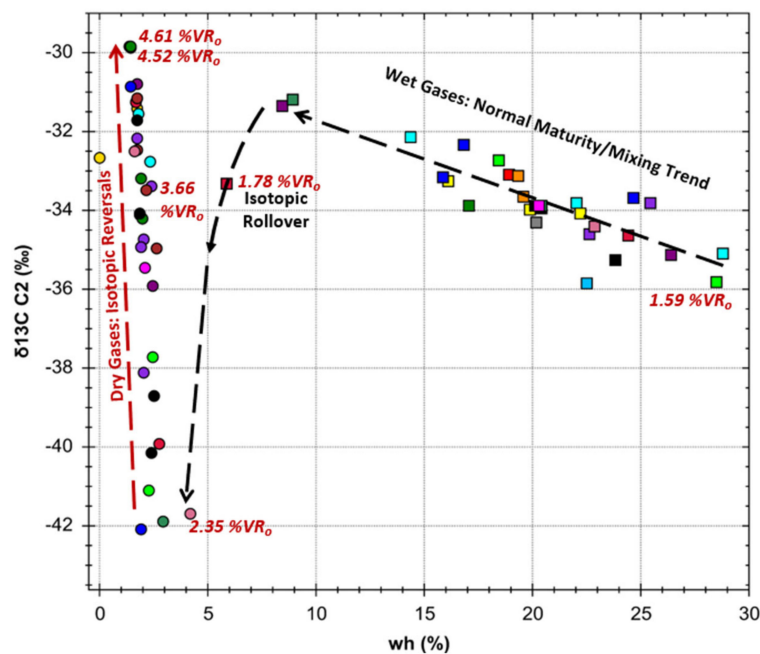


Figure 9. Plot of percent gas wetness (wh) against ethane $\delta^{13}C_2$ for Marcellus Formation produced natural gases. VR_o values noted next to selected data points were measured by Dr. Wayne Knowles, Stratum Reservoir. Dashed arrows show increasing maturity trends. Most wet gases follow a normal maturity trend with decreasing wetness accompanied by increasing $\delta^{13}C_2$. Isotopic rollover [41,42] occurs at a wetness of about 5.9% where decreasing wetness is accompanied by ^{13}C depletion. Isotopic reversals [37,38,42,43] begin at a wetness of 4% where the dry gases exhibit decreasing wetness accompanied by rapidly increasing $\delta^{13}C_2$.

4.2. Noble Gas Isotopic Analyses of Dry Gas Samples

Helium concentrations in a subset of gas samples collected from the dry gas-producing region range from 276.2 to 774.3 $\mu\text{cc/cc}$ for ^4He and 4.56 to 41.17 pcc/cc for ^3He (Table 4). Helium isotope ratios are reported relative to the atmospheric ratio $R_a = 1.4 \times 10^{-6}$ and

range from 0.011 to 0.071 R_a (Tables 3 and 4 and Figure 10a). $^4\text{He}/^{20}\text{Ne}$ ratios are between 76.8 and 11,704.3, which by comparison with the atmospheric $^4\text{He}/^{20}\text{Ne}$ ratio (0.188) shows that atmospheric helium contributions are negligible. Helium isotope ratios can therefore be considered as two-endmember mixing between crustal radiogenic helium (0.02 R_a) and minute contributions of ^3He -enriched mantle helium, for which sub-continental lithospheric mantle $^3\text{He}/^4\text{He}$ is 6.1 R_a [44–46]. $^3\text{He}/^4\text{He}$ ratios > 0.1 R_a are attributed to mantle fluid contributions [44]. Most of helium in the Marcellus Formation dry gases is derived from crustal radiogenic production (Figure 10a).

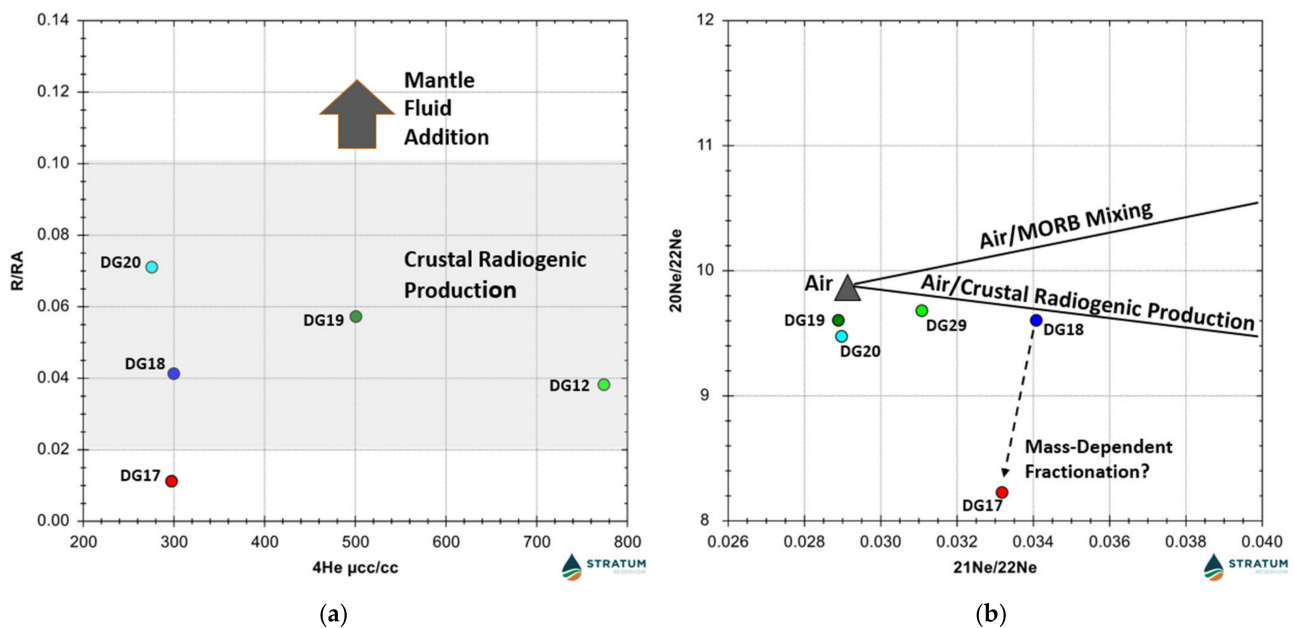


Figure 10. (a): Plot of ^4He concentration versus R/R_a for five selected dry Marcellus Formation produced gases collected in northeastern Pennsylvania (Table 4). (b) $^{21}\text{Ne}/^{22}\text{Ne}$ versus $^{20}\text{Ne}/^{22}\text{Ne}$ for the five Marcellus Formation dry gases samples.

Neon isotope ratios in the dry Marcellus Formation gases show a slight excess of radiogenically produced ^{21}Ne and/or ^{22}Ne relative to air, for which atmospheric $^{20}\text{Ne}/^{22}\text{Ne}$ is 9.81 and $^{21}\text{Ne}/^{22}\text{Ne}$ is 0.029 [45] (Figure 10b). $^{20}\text{Ne}/^{22}\text{Ne}$ in the Marcellus samples ranges from 8.223 to 9.674. $^{21}\text{Ne}/^{22}\text{Ne}$ is between 0.0289 and 0.0341. The samples mostly follow the crustal neon production-air mixing line, but scatter among some samples possibly reflects mass-dependent fractionation effects [44,46] (Figure 10b). Atmospheric ^{20}Ne concentrations range from 0.07 to 6.53 $\mu\text{cc/cc}$. The highest value is in the air contaminated DG19 sample and is considered anomalous and non-representative of Marcellus fluids.

Argon isotope ratios ($^{40}\text{Ar}/^{36}\text{Ar}$) show a modest excess of radiogenically produced ^{40}Ar , ranging from 315.69 to 404.1, compared with the air ratio of 298.6 [44–47]. Atmospheric ^{36}Ar is introduced into the subsurface dissolved in groundwater and in sediment pore water, and its concentration in the gas phase is controlled by solubility-dependent partitioning upon water-gas interaction. $^{40}\text{Ar}/^{36}\text{Ar}$ values in excess of the atmospheric ratio are due to contribution of radiogenic ^{40}Ar (designated $^{40}\text{Ar}^*$) produced by ^{40}K decay within the crust. The Marcellus $^{40}\text{Ar}/^{36}\text{Ar}$ ratios indicate variable additions of radiogenic $^{40}\text{Ar}^*$ to atmospheric, groundwater-derived Ar (Figure 11a). The $^4\text{He}/^{40}\text{Ar}^*$ ratios of the dry Marcellus gases indicate crustal production ratios reflecting very high thermal stress for the source material of the produced hydrocarbons (Figure 11b) [45–49].

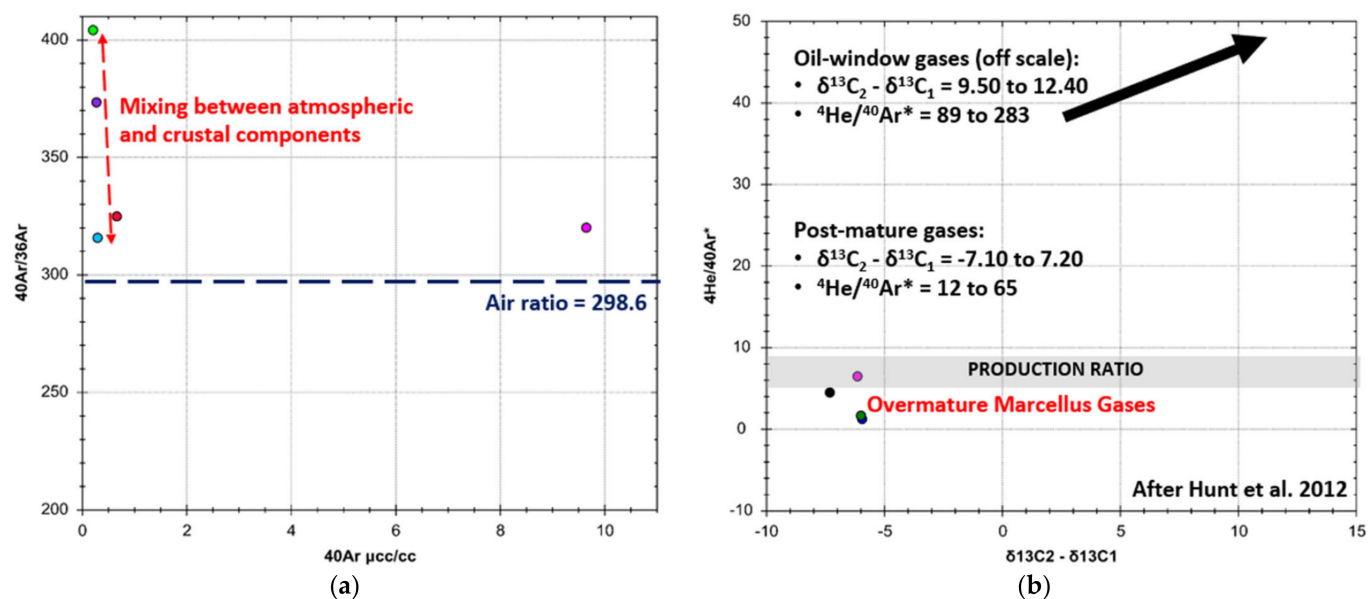


Figure 11. (a): ^{40}Ar concentration versus $^{40}\text{Ar}/^{36}\text{Ar}$ for five selected Marcellus Formation dry produced gases collected in northeastern Pennsylvania (Table 4). (b) $^4\text{He}/^{40}\text{Ar}^*$ versus $\delta^{13}\text{C}_2 - \delta^{13}\text{C}_1$ for the five selected dry gas samples (after Hunt et al. [50]).

Krypton and xenon abundances in the Marcellus Formation gas samples range from 11.1 to 231.9 ncc/cc and 0.6 to 17.5 ncc/cc, respectively (Table 4). Krypton and xenon ratios of gases produced from the DG17 and DG19 wells are indistinguishable from air and are slightly elevated relative to air in the DG12 and DG18 samples (Tables 4 and 5). In sample DG20, Kr abundance is enriched relative to Ar when compared to air or ASW values (Figure 12). ^{84}Kr and ^{132}Xe are fission products of uranium and their concentrations are dependent upon the uranium content of the crustal rocks. Previous studies suggest that excess Kr and Xe may be sourced from organic-rich shales themselves due to preferential sorption of the heavier noble gases onto clay or kerogen [47–49]. Figure 12 is a plot of $^{20}\text{Ne}/^{36}\text{Ar}$ against $^{84}\text{Kr}/^{36}\text{Ar}$ for dry Marcellus gases. Most of the gas samples lie near to the air and air-saturated water (ASW) values for $^{84}\text{Kr}/^{36}\text{Ar}$ indicating gas/water phase equilibrium. Three of the samples show variably high fractionation in $^{20}\text{Ne}/^{36}\text{Ar}$ suggesting that equilibration of groundwater with an earlier oil phase may have increased $^{20}\text{Ne}/^{36}\text{Ar}$ in the water phase [45,47]. One gas sample (DG20) exhibits high $^{20}\text{Ne}/^{36}\text{Ar}$ and extreme fractionation of $^{84}\text{Kr}/^{36}\text{Ar}$ (Figure 12). This may reflect release of atmosphere-derived Kr originally adsorbed and trapped in organic-rich sediment but might also indicate non-equilibrium diffusion or multiple stages of exsolution and dissolution [48,49].

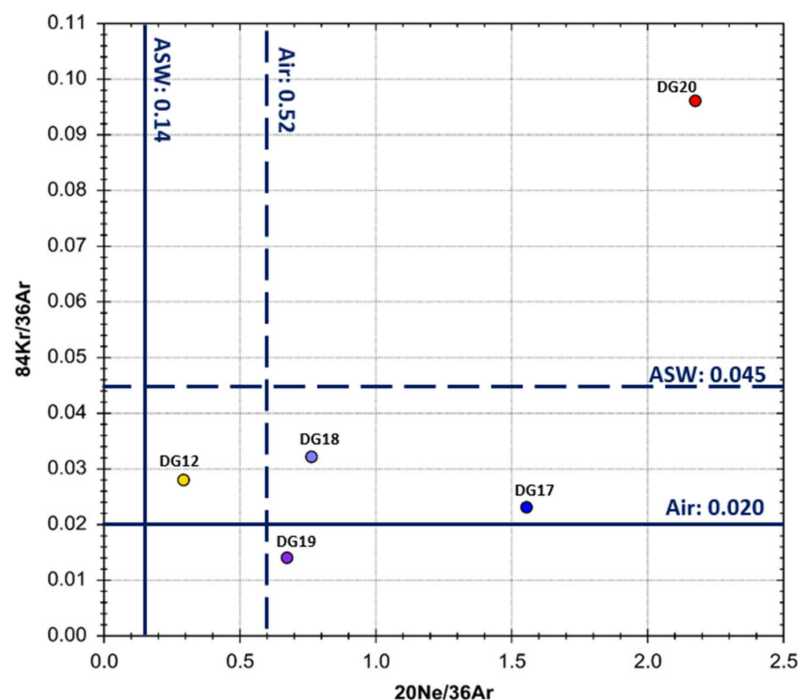


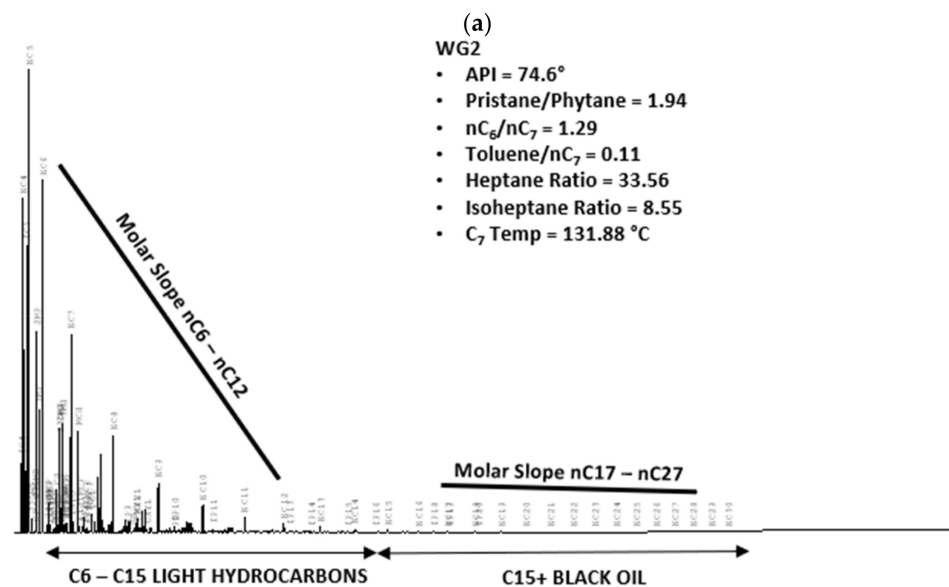
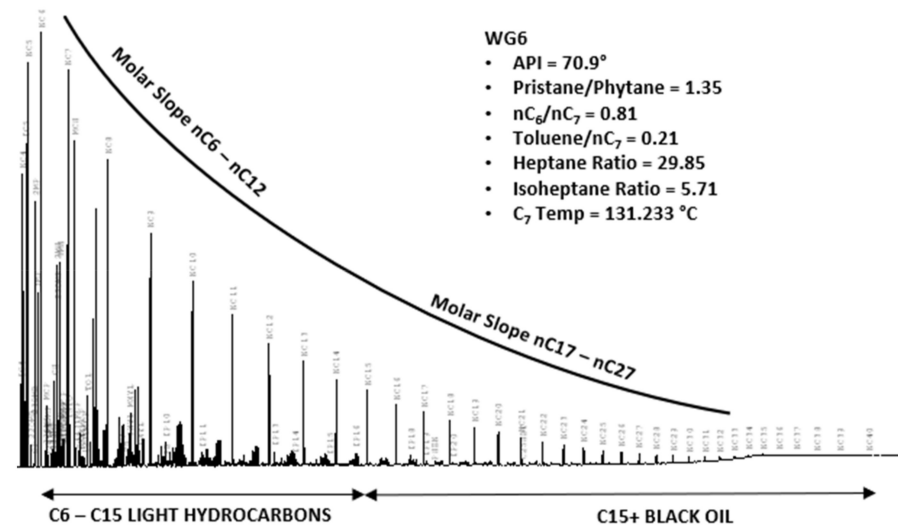
Figure 12. Plot of $^{20}\text{Ne}/^{36}\text{Ar}$ versus $^{84}\text{Kr}/^{36}\text{Ar}$ for five selected Marcellus Formation dry produced gases collected in northeastern Pennsylvania. Four of the gas samples lie near to air and ASW values for $^{84}\text{Kr}/^{36}\text{Ar}$ indicating gas/water phase equilibrium [44–47]. Samples DG17 and DG20 show higher fractionation in $^{20}\text{Ne}/^{36}\text{Ar}$. ^{20}Ne concentrations are strongly dependent on thermal maturity. Sample DG20 exhibits extreme fractionation of $^{84}\text{Kr}/^{36}\text{Ar}$ which may be due to release of atmosphere-derived Kr originally adsorbed and trapped in organic-rich sediment [48–50] or to non-equilibrium diffusion [51].

4.3. API Gravity and High-Resolution Gas Chromatography (HRGC) Analyses of Condensate Samples

The API Gravity of produced fluids measured in the wet gas region ranges from 57.8 to 74.6° (Table 6). All the samples are reported as condensate (>45° API) [52]. The condensates are dominated by light hydrocarbons mostly in the C_6 to C_{15} range. Figure 13 shows two HRGC chromatograms of condensates produced in the wet gas region. The WG6 condensate exhibits a unimodal n-alkane distribution with a maxima at $n\text{C}_6$ and resolvable hydrocarbons out to $n\text{C}_{40}$. The WG2 condensate also exhibits a unimodal n-alkane distribution, with maxima at $n\text{C}_5$, but GC peak responses are much diminished beyond $n\text{C}_{12}$ and the resolvable hydrocarbons only extend out to $n\text{C}_{30}$. All the produced condensate samples listed in Table 6 exhibit unimodal n-alkane distributions that vary between these two extremes with maxima between $n\text{C}_5$ and $n\text{C}_7$ and resolvable hydrocarbons between $n\text{C}_4$ and $n\text{C}_{40}$. Differences in the molar slopes of the light hydrocarbons ($n\text{C}_6$ – $n\text{C}_{12}$) and the black oil C_{15+} hydrocarbons ($n\text{C}_{17}$ – $n\text{C}_{27}$) observed on the HRGC chromatograms of the Marcellus samples (Figures 13 and 14) reflect various primary and secondary processes that affected the produced fluids such as maturity and thermal alteration, expulsion and migration, mixing, gas stripping, water washing, and plausibly production fractionation [53,54].

Thompson [55] developed several C_6 – C_7 ratios that are useful for describing light hydrocarbon distributions by compound class. A cross-plot of two of these ratios, the heptane and isoheptane ratios, is useful for assessing light oil maturity [56], including maturity of the Marcellus fluids (Figure 15a). The heptane and isoheptane ratios reflect the relative abundance of C_7 structural isomers in the fluid [55]. The heptane ratio of the WG6 condensate is 29.85 and its isoheptane ratio is 5.71 (Table 6). The respective heptane and isoheptane ratios of the WG2 condensate are 33.56 and 8.55 (Table 6). These ratios suggest that the condensates are so-called supermature light oils. The supermature classification indicates that all of the light Marcellus oils were thermally cracked [55]. The

fluids experienced protracted thermal transformation, i.e., ring opening, and substantial gasification (Figure 15a).



(b)

Figure 13. High resolution gas chromatograms of two produced condensates collected in the wet gas-producing region. The solid black lines illustrate the molar slope(s) [53] of n-alkane peak heights for light (nC_6 – nC_{12}) and C_{15+} hydrocarbons. These two chromatograms represent end member compositional extremes observed in Marcellus condensates in the basin. (a): The WG6 condensate exhibits a unimodal n-alkane distribution with a maxima at nC_6 , resolvable hydrocarbons out to nC_{40} , and a smooth transition of molar slope between light hydrocarbons and black oil. (b): The WG2 fluid shows has a maxima at nC_5 , but GC peak responses are much diminished beyond nC_{12} and there is a distinct break in the molar slopes of the light hydrocarbons and black oil.

BeMent et al. [57] and Mango [58] concluded that the ratio of 2,4-dimethylpentane/2,3-dimethylpentane in light oil corresponds to the temperature of petroleum generation and expulsion from organic matter in a source rock:

$$^{\circ}C_{7\text{TEMPERATURE}} = 140 + 15((\ln [2,4\text{-dimethylpentane}/2,3\text{-dimethylpentane}])). \quad (2)$$

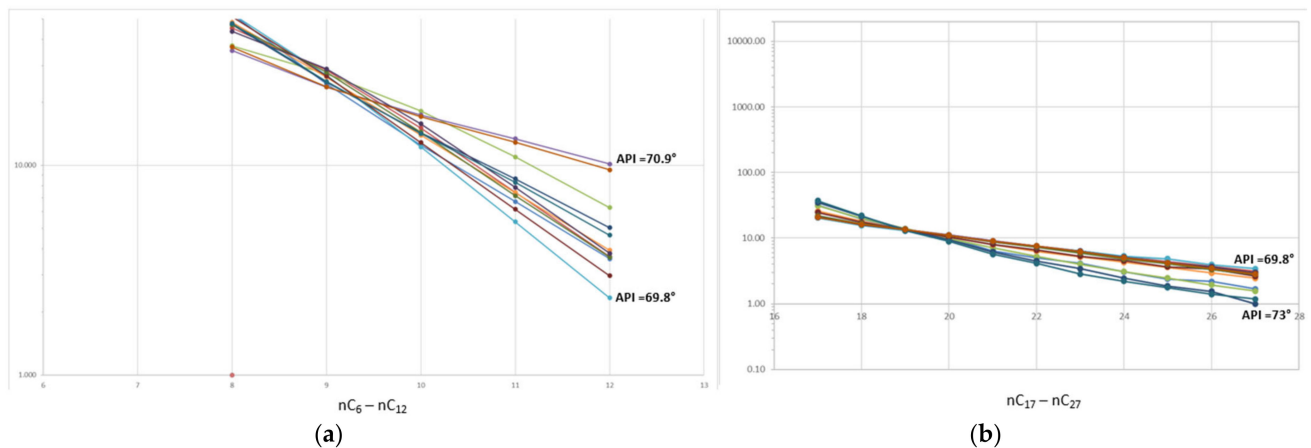


Figure 14. Normalized percent molar n-alkanes plotted against carbon number for Marcellus Formation condensates collected in the wet gas-producing region. % molar n-alkanes = $A \cdot e^{-B \cdot C_n}$ where A and B are regression factors used for correlation to oil parameters of interest (API, GOR, maturity) [51,52]. (a) nC_6 – nC_{15} alkanes. (b) nC_{17} – nC_{27} alkanes.

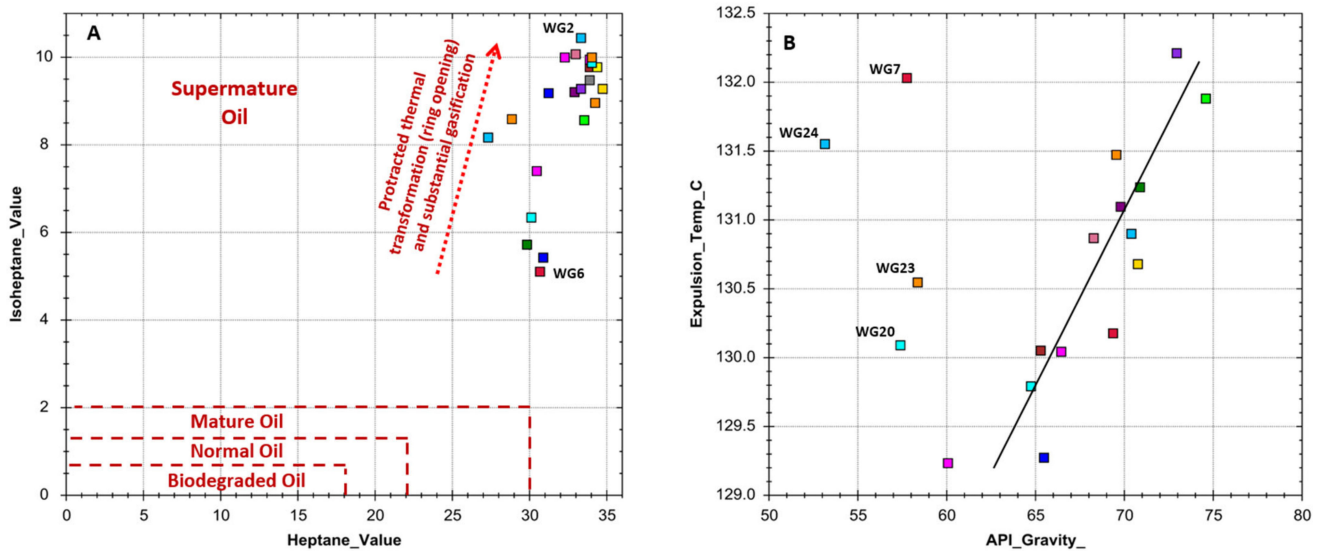


Figure 15. (A) Heptane ratio versus isoheptane ratio for Marcellus Formation condensates produced in the wet gas region. The heptane and isoheptane ratios reflect the relative abundance of C_7 structural isomers in the fluid [52]. (B) API gravity versus C_7 generation/expulsion temperature for Marcellus Formation condensates produced in the wet gas region. The API values of most condensates correlate with C_7 expulsion temperatures. The well ID (Table 6) of the four samples falling off of the correlation is shown next to the data point.

C_7 expulsion temperatures in the Marcellus Formation condensates range from 130 to 132 °C (Figure 15b) indicating late-mature hydrocarbons [52]. These temperatures are less than those indicated by post mature VR_0 values in the wet gas reservoirs (Figures 3 and 9). Accurate C_7 temperatures based on 2,4-dimethylpentane/2,3-dimethylpentane ratios are limited to a range of about 95 to 135 °C, the temperatures associated with intense generation and expulsion; subsequent thermal decomposition of oil expelled from parent kerogen into the pore space of the rock is unimportant [57,58]. I conclude that (1) primary Marcellus oils were mostly generated in the late oil window at burial temperatures of approximately 130 to 132 °C and subsequently (2) thermally cracked and altered to yield lighter hydrocarbons and gas. The API values of most condensates correlate with C_7 expulsion temperatures (Figure 15b).

The two plots of toluene/ nC_7 against nC_7 /methylcyclohexane (MCH) shown in Figure 16 suggest additional alteration processes in the Marcellus condensates. Toluene/ nC_7 is an aromaticity ratio and nC_7 /MCH is a paraffinicity ratio. Unaltered marine oils have toluene/ nC_7 between about 0.2 and 0.6 and nC_7 /MCH between 0.4 and 1.5 [55,56]. Toluene/ nC_7 in the Marcellus condensates is between 0.11 and 0.21 and nC_7 /MCH is between 1.12 and 1.87 (Figure 16). Most of the Marcellus Formation liquids produced in the wet gas region appear to have been stripped by gas, i.e., migrating gas dissolved light end alkanes into itself [54]. Furthermore, the plots in Figure 16 shows systematic depletion of soluble toluene accompanied by increasing nC_7 which suggests the hydrocarbons were affected by hydrodynamic flow and water washing [55]. Low concentrations of water-soluble benzene (0.62 to 1.19%) in the liquids support this interpretation [59]. Very low TR7 (1-trans-3-dimethylcyclopentane/1,1-dimethylcyclopentane) and TR8 (2-methylhexane + 3-methylhexane/2,2-DMP + 2,3-DMP + 2,4-DMP + 3,3-DMP + 3-ethylpentane) suggest migration and secondary alteration effects [59].

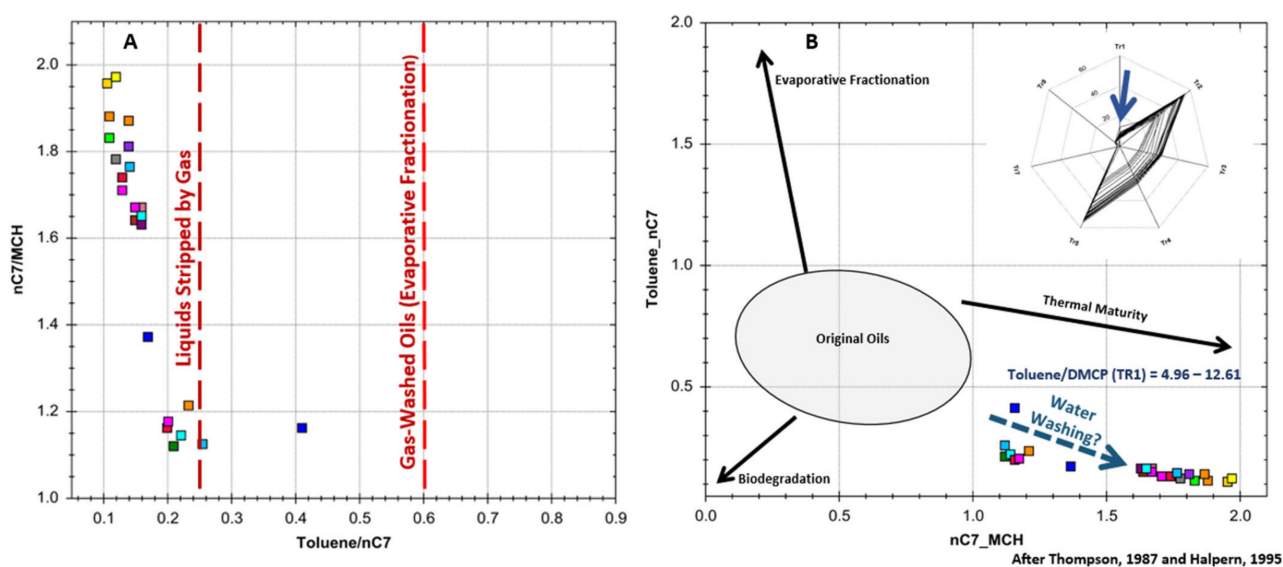


Figure 16. (A) Thompson [55] plot showing increasing evaporative fractionation (gas washing) can cause the residual liquid to be heavier and more aromatic (down and to the right) but the migrating gas will become more liquid rich (up and to the left). Here most of the Marcellus liquids appear to have been stripped by gas (dry gas picks up light hydrocarbons, i.e., the gas dissolves light end alkanes into itself [54]). (B) Halpern [59] interpretive plot shows low toluene/ nC_7 and systematically increasing nC_7 /MCH trends suggestive of water washing. This interpretation is supported by low toluene/DMCP (TR1 on the insert star plot), and very low amounts of benzene. Very low TR7 suggest migration and secondary alteration effects [59].

Figure 17 is a plot of C_7 expulsion temperature versus molar slope A (nC_{17} – nC_{27}) for the Marcellus condensates. The plot provides a comparison of the thermal maturities of the light hydrocarbons (nC_6 – nC_{12}) and the C_{15+} hydrocarbons in the oils. While a few samples follow the expected thermal maturity trend for normal unaltered oils, most samples plot up and to the left of that trend indicating mixing with higher maturity oil [54]. Most Marcellus Formation condensates produced in the wet gas region are mixtures of primary late-mature light oils cracked from kerogen and secondary liquids cracked from residual oils in the shales.

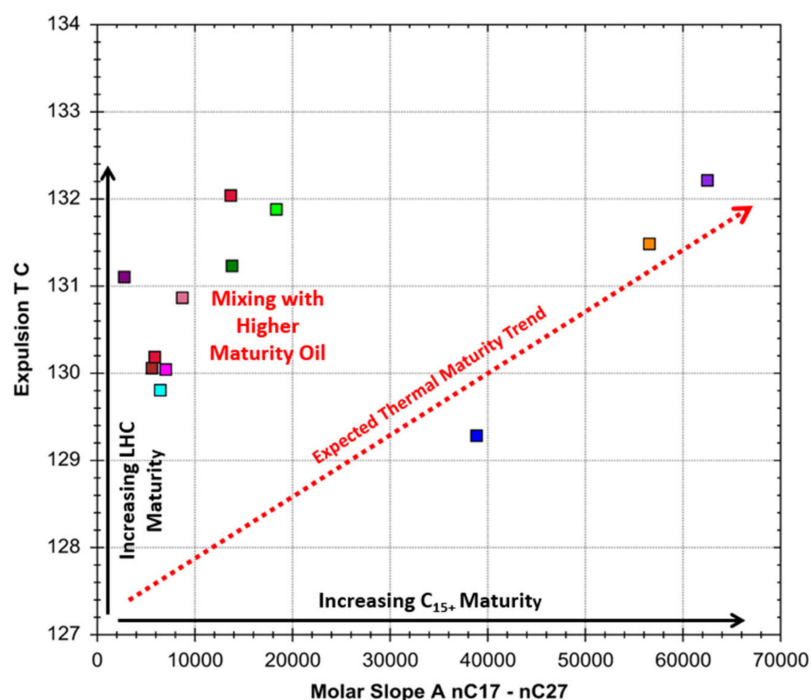


Figure 17. Plot of molar slope A for C_{15+} hydrocarbons against C_7 oil generation/expulsion temperature for Marcellus Formation condensates produced in the wet gas region (after Adams and Kornacki [54]). The plot indicates mixing of higher maturity light hydrocarbons (LHC) and variable maturity C_{15+} hydrocarbons.

4.4. Variations in Thermal Maturity of Marcellus Formation Hydrocarbon Gases

As stated earlier, condensate production in the basin is from reservoirs with reported VR_o of 1.0 to 2.8%. Dry gas production is from reservoirs with reported VR_o from 2.0 to >3.0%. While VR_o is considered a critical parameter for maturity assessment in the Marcellus play [1,11], it is a difficult value to accurately measure in these rocks [32]. Published vitrinite reflectance data and maps show VR_o contours ranging from 0.5% in western New York, northwestern Pennsylvania, and eastern Ohio to between 2.5 and 3.5% in eastern New York, northeastern Pennsylvania, western Maryland, and central/eastern West Virginia [2,32,33]. On these maps, wet gas production in western Pennsylvania and northwest West Virginia is bound by $VR_o = 1.0$ to 1.6% and dry gas production is bound by $VR_o = 2.0$ to 3.5% [2]. This contrasts significantly with the carefully sampled and measured VR_o completed for this study (Figures 3 and 4) and in published site-specific investigations [29–32]. Published burial history reconstructions indicate modeled VR_o of 1.3 to 1.8% in the wet gas region and 2.3 to 3.2% in the western part of the dry gas region [33,34]. Interestingly, reported measured VR_o in samples collected from the same modeled wells are 0.75 to 1% in the wet gas region and $\pm 2.0\%$ in the dry gas region [33]. These large reported VR_o discrepancies are due to numerous sources of error including sample type (core, cuttings, outcrop) and handling, contamination, lithology, and organic matter identification [32]. Organic matter in thermally post mature and overmature Marcellus Formation reservoirs consists mostly of a solid bitumen/pyrobitumen organic matrix with sparse inertinite (Figures 3 and 4) [12,30]. Vitrinite is largely absent or difficult to recognize and oil-prone kerogens have been converted to hydrocarbons (Figures 4 and 5) [30]. Consequently, many workers have endeavored to identify and utilize different geochemical proxies for rapid and practical maturity assessment during Marcellus reservoir development [12,30,32,60,61]. These include produced gas composition and stable gas isotopes [62–64].

Figure 18a is a popular maturity model from Whiticar [65] based on mathematical models published by Faber [66] and Whiticar [67]. This model grossly underestimates the actual thermal maturity of the Marcellus gases due secondary effects discussed below [65].

However, this plot of $\delta^{13}C_2$ versus $\delta^{13}C_3$ exhibits strong congruence for the gas isotopic values suggesting that the data do reflect thermal maturity [65,68,69]. Calculating distance between $\delta^{13}C_2$ and $\delta^{13}C_3$ of the Marcellus gas samples (Figure 18b) provides calibration of the carbon isotope correlation trends to measured and modeled maturity parameters.

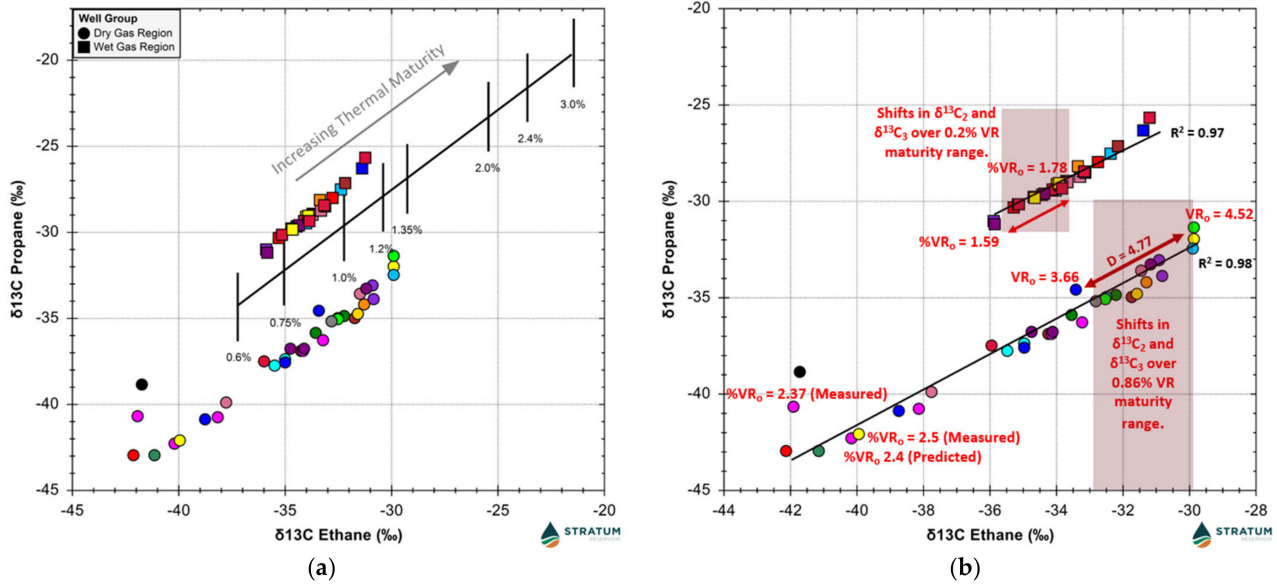


Figure 18. (a) Modeled vitrinite reflectance equivalents based on calculations published by Faber [66] and Whiticar [67]. (b) The same plot including calibration to actual VR_o measurements based on the distance calculated for the relevant $\delta^{13}C_2$ – $\delta^{13}C_3$ pairs (method suggested by Jennifer Adams, Stratum Reservoir, 2019 personal communication).

Figure 19a is a plot of methane $\delta^{13}C$ versus ethane $\delta^{13}C$. The trends for the wet and dry gas samples are again highly congruent although some scatter in $\delta^{13}C_1$ values suggests mixing of gases cracked from kerogen and gases cracked from oil (discussed further below). In this model, the wet gas maturities do approximate those observed in the Marcellus Formation organic matter. The dry gas data, however, shift away from the modelled maturity trends and lie within the field of a so-called super mature Type II kerogen source.

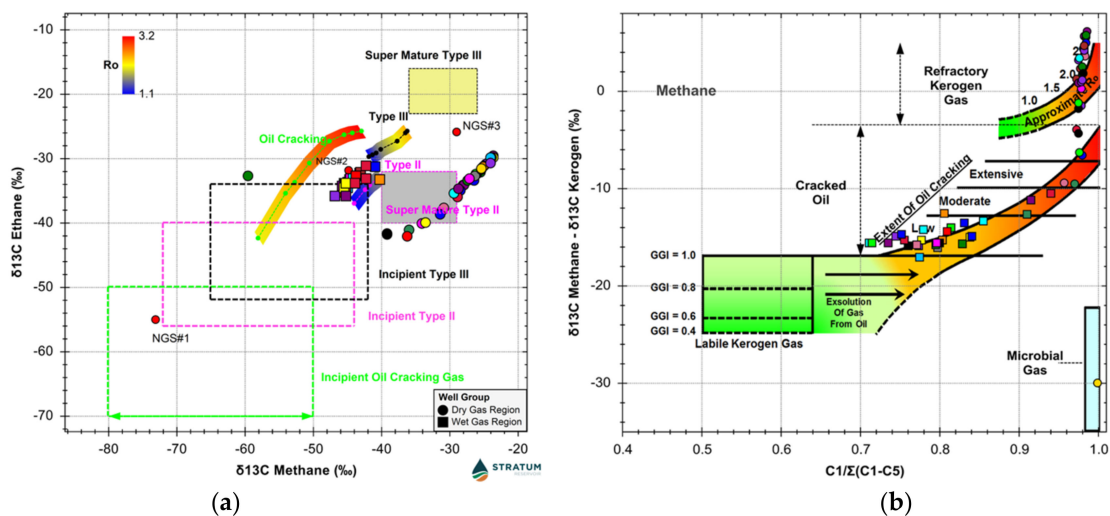


Figure 19. (a) Plot of methane $\delta^{13}C$ versus ethane $\delta^{13}C$ for produced Marcellus Formation natural gases. VR_o maturity trends after Rooney et al. [40]. NGS#1, NGS#2, and NGS#3 are natural gas standards employed during isotopic analyses of the Marcellus samples. Wet gases lie between the fields for late

mature gases generated from Type II oil-prone kerogen and postmature hydrocarbons generated by oil cracking. Dry gases plot within or near the fields of supermature (same as overmature and defined as $VR_o > 2.0\%$) hydrocarbons. (b) Clayton [68] plot of gas dryness ($C_1/\sum C_{1-C_5}$) versus the per-mil difference between methane and total source kerogen for produced Marcellus Formation natural gases. GGI is the Gas Generation Index, i.e., the ratio of total gas generated from labile (oil-prone) kerogen to the total gas generation potential of that kerogen. The wet Marcellus gases and some dry gases plot along a Rayleigh fractionation trend defined for hydrocarbons generated by oil cracking. Most dry gases plot congruently along a mixing trend between methane cracked from refractory kerogen and hydrocarbons derived from oil cracking. Note that one gas sample (DG19 in Table 1) plots in the microbial methane field.

Noble gas data also constrain the thermal maturity of dry gases collected in north-eastern Pennsylvania (Figure 11b and Table 5). Hunt et al. [50] demonstrated that post mature to overmature gases in the northern Appalachian basin have $\delta^{13}C_2-\delta^{13}C_1$ ratios of -7.10 to 7.20 and $^4He/^40Ar^*$ ratios of 12 to 65. The $\delta^{13}C_2-\delta^{13}C_1$ ratios of most Marcellus Formation hydrocarbons produced in the dry gas region are between -7.32 and -5.33 . Most Marcellus $^4He/^40Ar^*$ ratios range from 1.6 to 6.34, values within or below crustal noble gas production ratios due to high-temperature release of He, Ne, and Ar from the rocks [50]. $^{21}Ne/^40Ar^*$ ratios (1.06×10^{-5} to 2.18×10^{-5}) are below crustal production ratios as well [50].

4.5. Secondary Effects

Several secondary effects have altered the chemical composition and isotopic ratios of the produced Marcellus Formation gases. The documented range of carbon isotopic compositions of Marcellus organic matter suggests that some part of the range of isotopic compositions of the produced gases might be due to mixing of gases generated from kerogen with variable $\delta^{13}C$ (Figure 7). However, a plot of gas dryness against the per-mil difference between kerogen $\delta^{13}C$ and methane $\delta^{13}C$ (Figure 19b) indicates that all the wet gas samples and several of the dry gas samples were altered by incipient to extensive oil cracking in the wet gas window. This is consistent with the heptane and isoheptane ratios in the condensates discussed above (Figure 15a). Gases derived from oil cracking are isotopically heavier than gases derived directly from kerogen cracking and become heavier with increasing maturity due to Rayleigh fractionation [68]. Gas derived from oil cracking mixes with earlier-formed gas derived from kerogen cracking which remained dissolved in the oil undergoing cracking [68]. Thus, the methane $\delta^{13}C$ of the wet gas samples is a weighted average of the isotope ratio of the gas cracked from oil and earlier-formed gas cracked from kerogen [68,69]. Wet gas mixing and maturation trends are linear and highly congruent on the plots of methane $\delta^{13}C$ versus methane δD (Figure 20a) and methane concentration (Figure 20b). The C_2/C_3 ratios and difference between $\delta^{13}C_2$ and $\delta^{13}C_3$ in these samples are 2.1 to 4.4 and -4.62 to -4.97% , respectively, indicating secondary oil cracking [70]. Rayleigh-type fractionation should cause the isotope ratios of individual hydrocarbon components to be a linear function of the natural logarithm of the concentration as shown in Figure 21 [71,72]. Ethane isotope ratios of the wet gases plot on a straight line as a function of the inverse of concentration, indicating progressive depletion of $\delta^{13}C_2$ with decreasing concentration (Figure 21). Wet Marcellus gases are mixtures of residual associated gases generated in the late-oil window and post-mature hydrocarbons generated from oil cracking in the wet gas window.

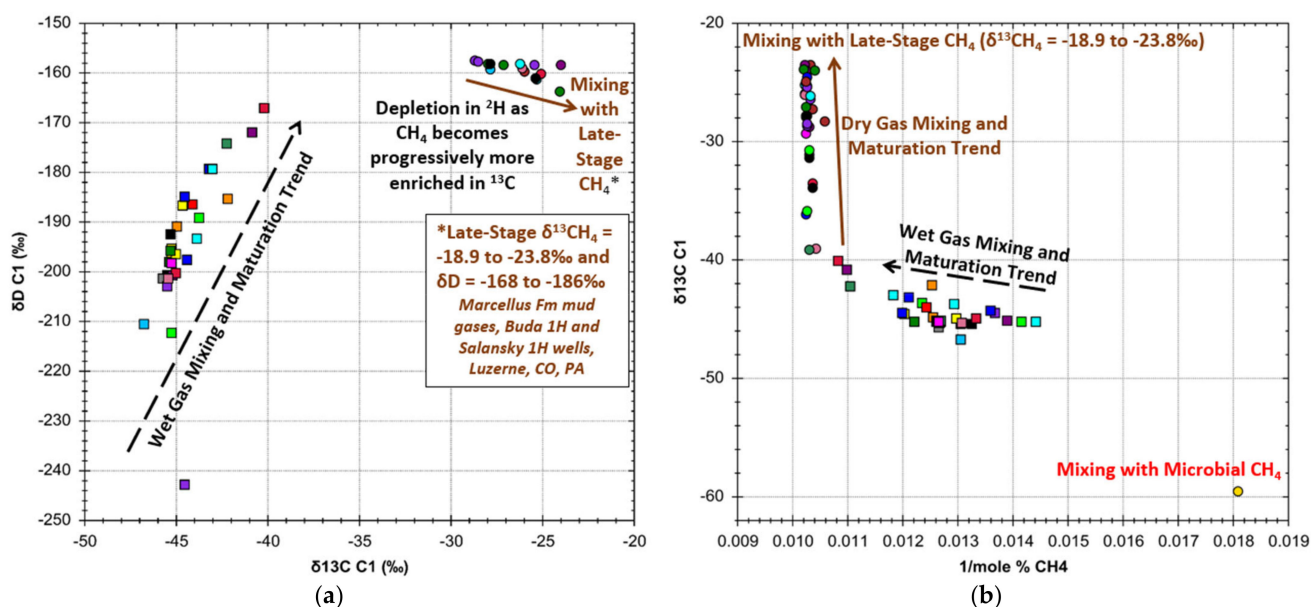


Figure 20. (a) Schoell plot [36] of $\delta^{13}\text{C}$ versus δD for methane in Marcellus Formation wet and dry gas samples from the Appalachian basin. Isotope compositions fall on two distinct trends. The wet gases (squares) plot along a mixing trend ($R^2 = 0.7$) showing progressive enrichment in ^{13}C and ^2H characteristic of a thermal maturation sequence [36]. The dry gases (circles) show depletion in ^2H as methane becomes progressively more enriched in ^{13}C ($R^2 = 0.67$). The extension of this trend to Late-Stage $\delta^{13}\text{CH}_4$ is discussed in the text. These two trends are identical to those published by Burruss and Laughrey [72] for Ordovician and Silurian gases produced from conventional and unconventional reservoirs in the basin. (b) Variation of methane isotopic composition with concentration in Marcellus Formation wet and dry gas samples. The wet gases fall along the maturation/mixing trend on the Schoell plot in 20a and along the Rayleigh fractionation trend for hydrocarbons generated by oil cracking shown in Figure 19b. The dry gases show a mixing trend consistent with the trend shown on the Schoell plot (20a) that extends to the Late-Stage CH_4 end member. These trends are also identical to those exhibited by wet and dry Ordovician and Silurian gases produced in the basin [72].

Most of the samples collected from the dry gas-producing region fall within the genetic field for methane cracked from refractory kerogen at VR_o equivalents of approximately 1.5 to $\geq 2.5\%$ on the plot of $\text{C}_1/\sum\text{C}_1\text{-C}_5$ versus the per-mil difference between methane and total source kerogen (Figure 19b). Actual thermal stress in these Marcellus rocks is much higher based on carefully measured VR_o , illite crystallinity, H/C and O/C ratios, noble gas data, and calibrated stable gas isotope ratios (Figures 3, 4, 11 and 18). Published mineral and fluid inclusion data indicate burial temperatures of 250–300 °C [30,72–77]. Lewan and Kotarba [78] experimentally demonstrated that primary gas generation from oil-prone and gas-prone kerogen and associated bitumen ends by a VR_o of 2.0% because no alkyl moieties remain to source hydrocarbons. Secondary gas generation from oil cracking occurs primarily between VR_o 1.7 and 2.9% [78]. Hydrocarbon gases already generated and trapped, however, can remain in the shales to much higher temperatures [78–80]. The productivity of Marcellus Formation reservoirs in the dry gas region is a function of shale reservoir properties (porosity, permeability, fluid saturations, rock mechanics) and hydrocarbon retention versus expulsion; productivity is not a function of thermal maturity [12,30,81,82]. The noble gas data listed in Table 3 support this interpretation. In Figure 22, mixing is evident between two atmosphere-derived end members, ^{20}Ne and ^{36}Ar . ^{20}Ne is highly fractionated. ^{36}Ar is non-fractionated. Atmospheric ^{36}Ar exhibits a negative correlation with $^{20}\text{Ne}/^{36}\text{Ar}$ (Figure 22). Gas collected from economically productive wells have high $^{20}\text{Ne}/^{36}\text{Ar}$. Gases sampled from poor producing wells with high water cut have low $^{20}\text{Ne}/^{36}\text{Ar}$ similar to unfractionated groundwater. Decreasing gas productivity and decreasing gas retention are correlated with decreasing $^{20}\text{Ne}/^{36}\text{Ar}$ (Figure 22).

Like the wet gases described above, the dry gas isotope ratios are cumulative so mixing of wet gas components generated by extensive oil cracking and methane derived from postmature refractory kerogen cracking is implied by the plot in Figure 19b [68]. The dry gas samples exhibit depletion in ^2H as methane becomes progressively enriched in ^{13}C (Figure 20a). This uncommon trend is also observed in deeper non-associated Silurian through Ordovician conventional and unconventional reservoir gases in the study area [72]. Burruss and Laughrey [72] suggested that isotopic exchange with formation water is one mechanism that could explain ^2H depletion in methane produced from these deeper reservoirs. Isotopic exchange with formation water is a possible mechanism for ^2H depletion in the dry Marcellus gases as well.

The isotopically heaviest methane measured in the Marcellus Formation to date, sampled from mud gases recovered from non-productive shale wells drilled in Luzerne County, Pennsylvania, has $\delta^{13}\text{C}_1$ between -18.9 and -23.8‰ and $\delta\text{D}_{\text{C}_1}$ between -186 and -166‰ [12]. The dry gas mixing and maturation plots in Figure 20 are reflective of mixing with this isotopically heavy, postmature late-stage methane derived from refractory kerogen. C_2/C_3 ratios in the dry gas samples are between 20.5 and 44.4, and the difference between $\delta^{13}\text{C}_2$ and $\delta^{13}\text{C}_3$ is between 2.41 and 1.44‰ indicating secondary gas cracking [70]. The dry gas samples exhibit Rayleigh fractionation trends consistent with ethane and propane destruction during secondary gas cracking accompanied by redox reactions [72] (Figure 21).

One of the dry gas region samples (DG19) has an unusually light methane $\delta^{13}\text{C}$ of -59.58‰ indicating a microbial gas component (Figures 6, 7 and 19b). Ethane $\delta^{13}\text{C}$ is -37.2‰ . The gas is a mix of microbial and thermogenic hydrocarbons. This sample has unusually high crustal ^{40}Ar ($3088.4 \mu\text{cc/cc}$) and relatively high atmospheric ^{36}Ar ($9.65 \mu\text{cc/cc}$) compared to other noble gas concentrations in this region (Table 4 and Figure 22). The high ^{36}Ar concentration suggests recent interaction with atmospheric gases [44–47]. This sample has a $^{20}\text{Ne}/^{36}\text{Ar}$ ratio of 0.677 which approximates the upper limit for single-stage equilibrium for fractionation between groundwater and gas [44–47] (Figure 22). The sample also contained 17.2 mole% hydrogen suggesting hydrolysis and casing corrosion.

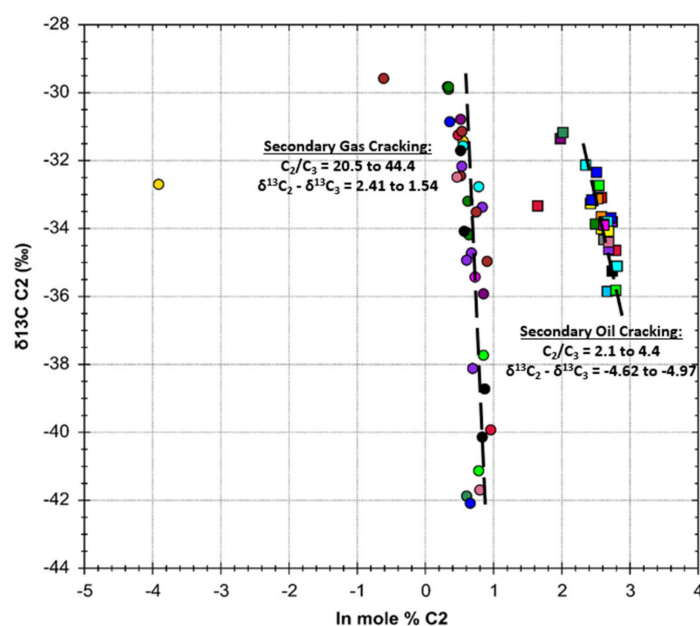


Figure 21. Evidence for mixing and Rayleigh fractionation secondary effects on ethane in Marcellus Formation gases. The isotopic composition of ethane in both the wet and dry gases is a linear function of the natural logarithm of the concentration indicating Rayleigh fractionation [71,72]. Wet gases (squares) exhibit chemical and isotopic compositions consistent with oil cracking [70]. Dry gases (circles) exhibit compositions consistent with secondary gas cracking [70].

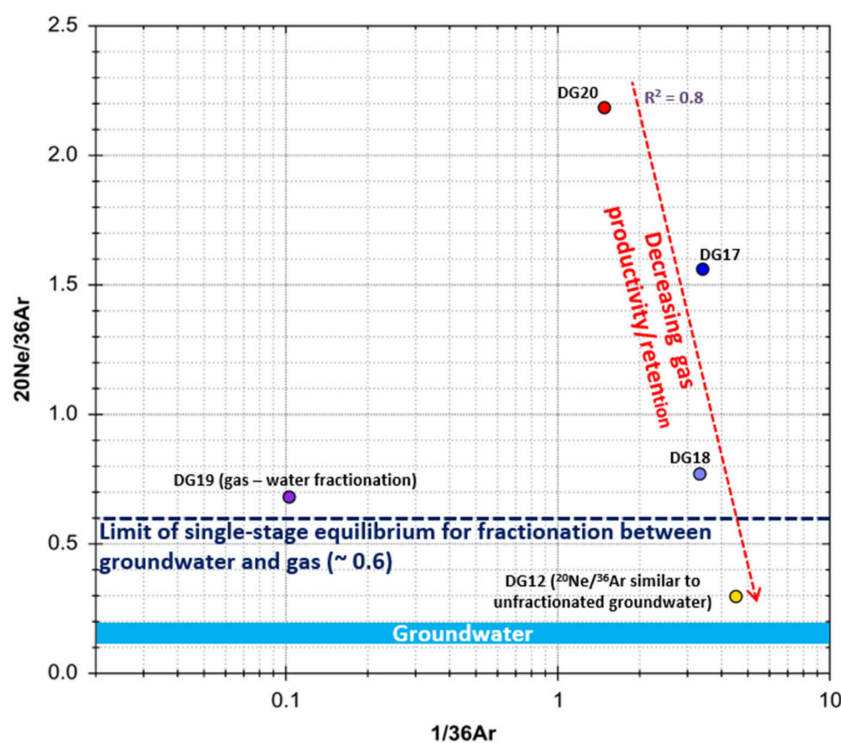


Figure 22. $^{20}\text{Ne}/^{36}\text{Ar}$ versus the reciprocal of ^{36}Ar concentration in five Marcellus dry gas samples. Mixing is evident between the two atmosphere-derived end members, one highly fractionated and the other non-fractionated. DG12 $^{20}\text{Ne}/^{36}\text{Ar}$ is similar to unfractionated groundwater. DG19 and DG18 have elevated $^{20}\text{Ne}/^{36}\text{Ar}$ which plot near the upper limit for single-stage equilibrium for fractionation between groundwater and gas (~ 0.6) [44–47,51]. DG17 and DG 20 have unusually high $^{20}\text{Ne}/^{36}\text{Ar}$ [45,47]. Excepting DG19 sample, atmospheric ^{36}Ar exhibits a negative correlation with $^{20}\text{Ne}/^{36}\text{Ar}$ ($R^2 = 0.8$). Hunt and others [50] observed this negative correlation in other northern Appalachian natural gases, including Marcellus Formation gas. They noted that a negative correlation exists between ASW ^{36}Ar as $^{20}\text{Ne}/^{36}\text{Ar}$ approaches solubility, indicating the diffusion of Ne as fluids migrate. The DG19 gas is altered by mixing with secondary microbial CH_4 , and by apparent hydrolysis/corrosion. The high ^{36}Ar (9.65 $\mu\text{cc}/\text{cc}$) likely reflects recent interaction with atmospheric gases.

4.6. Isotopic Reversals: Origin and Significance

Experimental and field evidence indicates that most terrestrial thermogenic hydrocarbons have so-called normal $\delta^{13}\text{C}$ and δD alkane patterns such as those exhibited by Marcellus Formation samples collected from the wet gas-producing region [37–40] (Figures 7a and 8). This normal pattern, with $\delta^{13}\text{C}_1 < \delta^{13}\text{C}_2 < \delta^{13}\text{C}_3$ and so on, and $\delta\text{D}_{\text{C}1} < \delta\text{D}_{\text{C}2} < \delta\text{D}_{\text{C}3}$ and so on, is the result of kinetic isotope fractionation in which the lighter carbon and hydrogen isotopes are more reactive than their heavier counterparts and take part in petroleum-generating reactions more readily [39,40]. Terrestrial hydrocarbons generated at high temperatures and pressures deeper within the crust, however, can have reversed $\delta^{13}\text{C}$ and δD patterns [62,63,72,83–92]. Marcellus gases in the dry gas-producing region of the basin exhibit reversed patterns (Figures 7b and 8).

The origin of isotopic reversals in dry gas is a controversial topic [85–100]. Reversed thermogenic $\delta^{13}\text{C}$ and δD alkane patterns have been interpreted as diagnostic evidence for:

1. Mixing of different sources of alkanes or of hydrocarbons generated from the same source at different levels of thermal maturity [62,63,83–87];
2. A combination of mixing with either Rayleigh fractionation (for carbon isotopes) or the exchange of methane hydrogen with formation water [72];
3. Destruction and subsequent reformation of C_{2+} alkanes via gas-phase radical recombination reactions at high temperatures and pressures [90];

4. Depletion of ^{13}C in residual ethane and propane as their molar fractions decrease during thermal decomposition [94];
5. Diffusive gas leakage [95];
6. Water reforming followed by Fischer–Tropsch synthesis [96];
7. Carbon exchange at high temperature [97];
8. Aerobic and anaerobic microbial oxidation of select alkane components [98];
9. Thermochemical sulfate reduction [99];
10. Isotopic fractionation during desorption from uplifted and de-pressurized late-mature shale resulting in isotope reversals in residual gas [92]; and
11. Hydrogen and carbon isotope distributions reflecting thermodynamic equilibrium either at the conditions of gas formation or during reservoir storage [100].

Two of these proposed mechanisms for generating isotopic reversals, microbial oxidation and thermal sulfate reduction, can be ruled out for the dry Marcellus gases based on geologic setting. Diffusive gas leakage is eliminated as a possible mechanism because the Marcellus reservoirs produce both isotopically heavy hydrocarbons and enriched light noble gases [50]. The Marcellus $^4\text{He}/\text{CH}_4$ ratios (283.1 to 907.6) are consistent with in situ Marcellus reservoir gases [8]. While C_{2-4} alkane synthesis from methane during gas-phase radical recombination reactions at high temperatures and pressures, resulting in isotopic reversals, has been demonstrated experimentally and for some abiogenic hydrocarbon reservoirs [88–91], maximum burial temperatures for the Marcellus Formation in northeast Pennsylvania fall short of those needed for these reactions [91]. Any argument for water reforming followed by Fischer–Tropsch synthesis remains equivocal because supporting carbon isotope measurements for CO_2 are mostly lacking in this dataset. The $\delta^{13}\text{C}_{\text{CO}_2}$ of the DG12 and DG19 gas samples (-26.5‰ and -31.8‰ , respectively) suggest that hydrocarbon oxidation might have affected these gas samples so might support such an interpretation [38,96]. However, mud gas $\delta^{13}\text{C}_{\text{CO}_2}$ of wells in the study area are between -19.7‰ and -10.2‰ , values more indicative of kerogen decarboxylation and high thermal stress [36–38].

Depletion of ^{13}C in residual ethane and propane during thermal decomposition [94] is a plausible hypothetical explanation for the carbon isotopic reversals observed in the Marcellus dry gas samples. However, the hydrogen isotope reversals (Figure 8) and variable, but significant, concentrations of atmospheric noble gas components (^{20}Ne , ^{36}Ar , ^{84}Kr) in the produced gases provide strong supporting evidence for the role of water-involved reactions in generating the isotope reversals [44–47,50,51,72,100].

Carbon and hydrogen isotopic reversals in the dry Marcellus Formation gases resemble those described by Burruss and Laughrey [72] for deeper Silurian and Ordovician conventional and unconventional reservoirs in northeastern and north-central Pennsylvania and south-central New York state. As in those deeper reservoirs, mixing combined with Rayleigh fractionation for the carbon isotopes (Figures 20 and 21) and the exchange of methane hydrogen with formation water for the hydrogen isotopes provides a plausible model for the Marcellus isotope reversals shown in Figures 7b and 8. Methane δD in the dry Marcellus gas samples ranges from -163.9 to -157.7‰ (Figure 8). Produced Marcellus brines in the dry gas region have reported δD between -49.1 and -41.5‰ [101]. Methane δD is depleted by approximately -118.8‰ relative to co-produced water. Methane equilibrated with formation water of the reported isotopic composition should have δD compositions of about -183‰ to -160‰ assuming maximum burial temperatures of 250 to 300 °C [72,102]. Measured δD in the dry Marcellus gas samples has this composition (Figures 6b and 20a; Table 1). The noble gas data discussed above indicate gas/water phase equilibrium for most Marcellus dry gases (Figure 12). Whyte and Darrah [103] argued that hydrocarbon isotope reversals are generated in relatively closed systems that retain greater amounts of ASW noble gas components as observed in the Marcellus gases and in the deeper Silurian and Ordovician fluids in the study area [72]. Finally, experimental work published by Gao et al. [104] demonstrated that water facilitates secondary cracking

of C_{2+} hydrocarbons to methane, possibly via a hydrated surface with catalytic activity, thus supporting the Burruss and Laughrey [72] model for isotopic reversals.

Milkov et al. [92] examined a comprehensive global data set of shale-gas composition and isotope data and observed that samples with carbon isotope reversals generally occur in onshore shale plays with overmature organic matter that underwent significant tectonic uplift. They hypothesized that isotope fractionation during desorption induced by significant basin inversion and depressurization of overmature shale source rocks leads to carbon isotope reversals. They concluded that the amount of uplift and associated depressurization is more important to creating isotopic reversals than thermal maturity in shale plays. Milkov et al. [92] noted that produced Marcellus gases with isotopic reversals occur in areas with 3 to 5 km of uplift and VR_o between 2 and 4% while produced Marcellus gases without reversals occur in areas with 1 to 2 km of uplift and VR_o between 1 and 2%. Milkov et al.'s samples without reversals are from wells completed along the up-dip margins of the Appalachian basin in western and central New York and in northwestern and western Pennsylvania [86,92,105]. The Marcellus wet gas samples without reversals in this paper's data set (Figure 7a) are from deeper locations that experienced ~1.04 to 2.4 km of erosion and uplift, have maturities of 1.59 to 1.78% VR_o , and are within the boundaries of the Rome Trough, a northeast-trending graben that is one of the major Cambrian interior rift system elements that extends into the Appalachian foreland basin [106]. In addition to burial temperatures, the thermal history of Devonian black shales within the Rome Trough was affected by excess heating connected to hot brine migration within the structure [107]. Marcellus dry gas samples with reversals in this paper's data set are from locations that experienced ~2.6 to 2.9 km of erosion and uplift and have maturities of 2.35 to 4.61% VR_o . The Marcellus gases without reversals in this paper's data set fall within the maturity parameters of such gases as defined by Milkov et al. [92] but experienced greater uplift. The Marcellus gases with reversals in this paper's data set are within the maturity range of such gases as defined by Milkov et al. [92] but experienced somewhat less uplift than those classified as reversed by those authors. However, uplift in the dry gas region was more rapid than in other parts of the basin and was accompanied by more rapid post-Alleghenian cooling and unroofing [108].

The Milkov et al. [92] hypothesis is compelling, particularly because it is based on a large global data set. However, the Marcellus produced gas isotope data do not entirely support their conclusion that uplift and associated depressurization is more important than thermal maturity for generating isotopic reversals in shale plays. In Figure 7b, the gases produced from Marcellus Formation shale with $VR_o = 2.37\%$ exhibit partial reversals with $\delta^{13}C_1 > \delta^{13}C_2 < \delta^{13}C_3$. Uplift and erosion amounted to ~2.6 km at this well location (WVDG1 and WVDG2 in Upshur County, WV) [33,34]. All of the remaining dry gas samples exhibit full carbon isotopic reversals, with $\delta^{13}C_1 > \delta^{13}C_2 > \delta^{13}C_3$, with the $\delta^{13}C$ of each gas component essentially increasing in parallel with increasing VR_o without any significant change in slope (Figure 7b). Furthermore, gas accumulations in Middle and Upper Devonian conventional sandstone reservoirs sourced by the Marcellus shale exhibit partial to full carbon isotopic reversals in several different parts of north central and western Pennsylvania, most of which experienced ≤ 2 km of uplift and erosion [7,62,109,110]. Petroleum generation and expulsion in Marcellus source rocks, and migration/accumulation in these conventional reservoirs occurred between ~359 and 225 Ma [33] suggesting that the isotopic compositions of the conventional reservoir gases are cumulative [66,69]. Combined oil and gas geochemical systematics of Marcellus-Upper Devonian sandstone petroleum system elements in Bradford County, Pennsylvania show carbon isotope reversals generated in-situ in a conventional Lock Haven Formation reservoir due to mixing of primary hydrocarbons and secondary gases from oil cracking [111]. Finally, comparisons of $\delta^{13}C_{1-3}$ variations observed during laboratory degassing of Marcellus pressure core with time-lapse production gas isotopic measurements (discussed below) contradict the hypothesis that molecular and isotopic fractionation during desorption after depressurization (from uplift and production

fractionation) is the principal mechanism causing isotopic reversals in the Marcellus dry gas reservoirs.

Thiagarajan et al. [100] proposed that C_{2+} n-alkane gases are initially produced by irreversible cracking chemistry, but, as thermal maturity increases, the isotope distribution of these species approaches thermodynamic equilibrium, either at the conditions of gas formation or during reservoir storage. They argue that at higher maturities the conversion of C_{2+} -rich wet gas to methane-dominated dry gas is controlled by thermodynamic conditions (temperature, fO_2 , and fH_2). In this model, the spatial and temporal distributions, and chemical/isotopic compositions, of major gas components and their breakdown products are controlled by their relative thermodynamic stabilities. Highly mature gases ($VR_o > 2\%$) such as the dry Marcellus fluids attain thermodynamic equilibrium. Turner et al. [112] concurred showing that (1) thermogenic gases may form in hydrogen isotopic equilibrium with co-occurring formation water and (2) CH_4 - CO_2 carbon isotopic equilibrium is a function of temperature in thermogenic shale-gas settings. Isotopic reversals observed in both unconventional and conventional reservoirs may be a function of quasi-equilibrium chemistry [100,112]. Modeled gas mixing in combination with Rayleigh fractionation and methane hydrogen exchange with formation water (Figures 20 and 21) is useful for describing isotopic enrichment or depletion as material moves between reservoirs in an equilibrium process and is consistent with these recently proposed thermodynamic equilibrium models.

Although the actual mechanism (or mechanisms) responsible for isotopic reversals in natural gases are debatable and consensus remains elusive, plots of $\delta^{13}C$ ratio distributions in reversed gases such as those shown in Figure 7b have pragmatic utility for identifying and mapping economic production limits in deep basins [72].

4.7. Stable Isotope Systematics of Marcellus Formation Shale-Gas during Pressure Core Degassing and Production

Unconventional shale-gas and shale-oil core delivered to the surface in pressurized sealed containers, which maintain formation pressure, facilitate direct gas-in-place measurements in the laboratory [113,114]. The cores are drilled under reservoir pressure and lifted to the surface without any loss of reservoir gas during transit. Controlled release of pressurized core samples in the laboratory permits accurate measurements of gas volumes extracted from natural high-pressure mudrocks. This laboratory procedure also provides an opportunity to collect a time-lapse series of reservoir gas chemical and isotopic analyses to document geochemical changes that occur during degassing of the core samples. Degassing is defined as expulsion of both gas phase and adsorbate phase gas molecules from the rock matrix [115]. These data reveal diagnostic geochemical trends that systematically vary with degassing time and cumulative hydrocarbon yield. Should such laboratory data anticipate gas compositional and isotopic variations during production, then they might provide useful predictive information about well performance over the operational life of the well [113].

The Marcellus pressure core samples listed in Table 3 provided a time-lapse data set of carbon isotopic measurements that document changes that occurred during degassing of the rock. Methane $\delta^{13}C$ measured during direct gas-in-place analysis of the Marcellus pressure core shows changes that vary systematically with cumulative degassing volume (Figure 23a). Initially, the methane became depleted in ^{13}C with increasing degassing time with a corresponding negative shift in ^{13}C of 1.38‰ at ~34% cumulative degassing volume. This early fractionation was due to the drop in partial pressure and the diffusivity difference of the isotopologues [115]. Adsorption/desorption within the reservoir pores was coupled with diffusion and delayed mass transport. ^{12}C was preferentially desorbed. This trend was followed by enrichment in methane ^{13}C beginning at approximately 40% of the cumulative degassing volume. Enrichment in $^{13}C_1$ continued with increasing degassing time with a positive isotope shift of 2.05‰ by 75.35% of the cumulative degassing volume. $\delta^{13}C$ increased towards the carbon isotope composition of crushed gas, i.e., gas liberated

from the shale by mechanical crushing at the end of the degassing experiment. Methane concentration of the crushed gas sample was 0.794 mole% and the final observed positive shift in ^{13}C towards the crushed gas was 4.88‰.

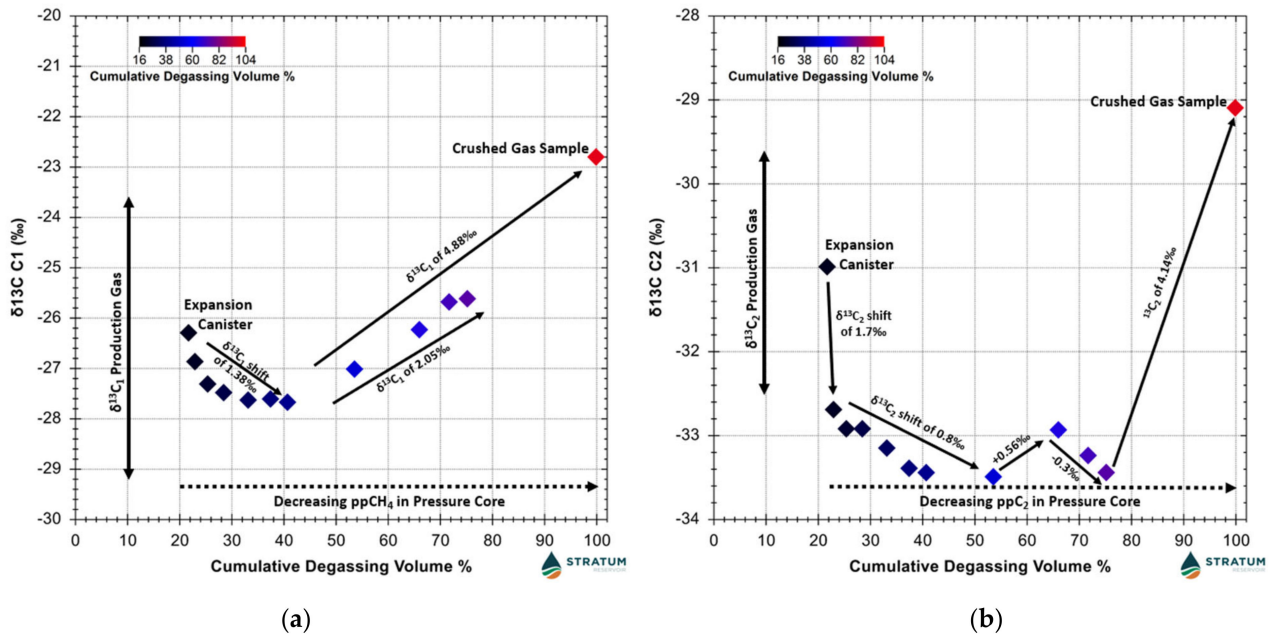


Figure 23. (a) Methane $\delta^{13}\text{C}$ versus cumulative degassing volume for Marcellus Formation pressure core compared with the range of produced gas $\delta^{13}\text{C}_1$ in adjacent wells in Susquehanna County, Pennsylvania. (b) Ethane $\delta^{13}\text{C}$ versus cumulative degassing volume for Marcellus Formation pressure core compared with the range of produced gas $\delta^{13}\text{C}_2$ in adjacent wells in Susquehanna County, Pennsylvania.

Ethane and propane $\delta^{13}\text{C}$ showed very different variations during direct gas-in-place measurements of Marcellus pressure core mostly due to increasing adsorption affinity from C_1 to C_3 . The pattern of ethane $\delta^{13}\text{C}$ variation was, at first, similar to that of methane (Figure 23a,b). The initial ethane $\delta^{13}\text{C}$ of -31‰ approximated the median $\delta^{13}\text{C}_2$ of production gases in the region, but rapidly decreased to -33.5‰ by 53.53% of the cumulative degassing volume (Figure 23b). This decrease was followed by a small positive $\delta^{13}\text{C}$ shift of 0.56‰ at 66.03% of the cumulative degassing volume before it resumed a decreasing $\delta^{13}\text{C}$ trend with increasing cumulative degassing volume. However, the ethane $\delta^{13}\text{C}$ of the crushed gas sample was -29.1‰ , a positive shift of 4.14‰ from the final degassing sample measured at 71.81% cumulative degassing volume. Propane $\delta^{13}\text{C}$ initially decreased by 0.3‰ between 22.93 and 25.47% of the cumulative degassing volume before exhibiting significant ^{13}C enrichment between 28.45 and 37.52% of the cumulative degassing volume, with a positive shift of 2.8‰ (Figure 24a). Propane $\delta^{13}\text{C}$ then decreased to -35‰ at 40.69% of the cumulative degassing volume followed by steady ^{13}C enrichment until the end of the degassing experiment. The crushed gas $\delta^{13}\text{C}$ of -34.7‰ is consistent with the average propane $\delta^{13}\text{C}$ of 34.9‰ in the immediate field vicinity.

Diffusion and desorption are the principal processes affecting the carbon isotope ratios of the Marcellus pressure core samples during laboratory degassing measurements. The variable direction and magnitude of isotope fractionations in the shale-gas samples during degassing are a function of these secondary processes. The plots in Figures 23 and 24 support the model predictions of Xia and Tang [115] who postulated that large isotopic fractionation due to gas transport would be observed under laboratory conditions with significant degassing.

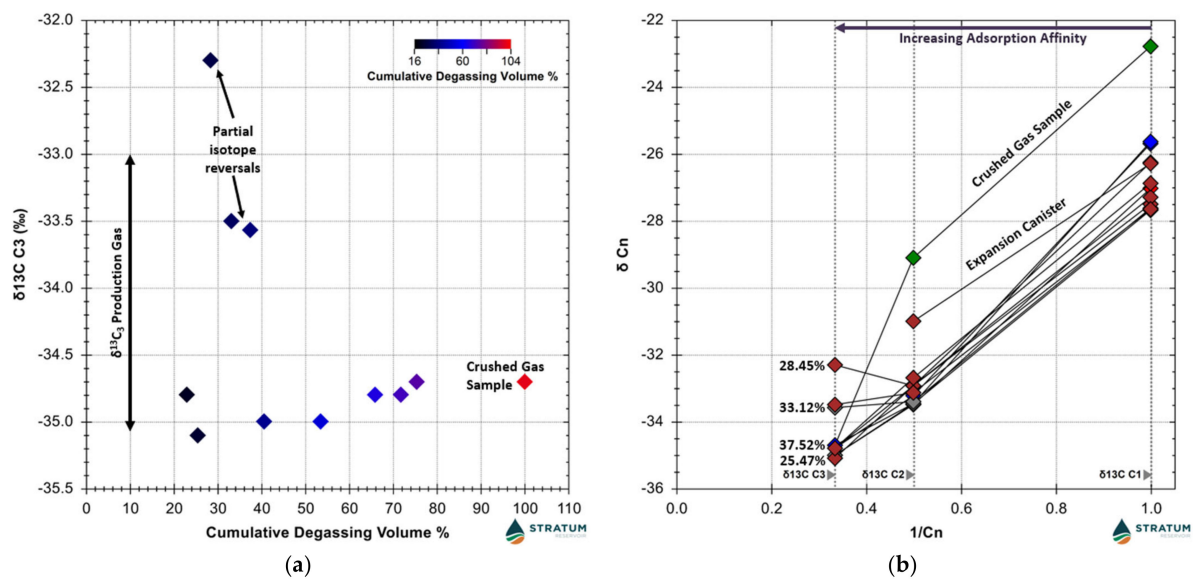


Figure 24. (a) Propane $\delta^{13}\text{C}$ versus cumulative degassing volume for Marcellus Formation pressure core compared with the range of produced gas $\delta^{13}\text{C}_3$ in adjacent wells in Susquehanna County, Pennsylvania. (b) Natural gas plot of twelve Marcellus Formation pressure core degassing samples. The $\delta^{13}\text{C}$ values for the gas components $\delta^{13}\text{C}_n$ ($n = 1-3$) are plotted as a function of $1/n$, where n is the number of carbon atoms in the molecule [39]. The non-linear fit of the data indicates a mixture of source inputs, gas derived from heterogeneous organic matter, or chemically altered gas [40]. Numbers plotted next to four of the propane $\delta^{13}\text{C}$ data points are cumulative degassing volumes (% of total).

The natural gas plot of the pressure core carbon isotope results reflects these secondary processes as well as those inherent in the Marcellus reservoir prior to drilling. The plot exhibits both partial and full carbon isotope reversals, with mostly non-linear trends (Figure 24b). The fully reversed natural gas plots of most of the pressure core degassing samples align with those of production gases in the study area (Figure 7b). However, there are three exceptions to this generalization. First, the ethane $\delta^{13}\text{C}$ of the initially released expansion canister gas is distinctly enriched in ^{13}C compared to all the other pressure core samples. There was insufficient propane in this sample for isotopic analysis. Second, propane in three of the degassing samples is enriched in ^{13}C compared to the other samples and consequently exhibits partial carbon isotopic reversals with $\delta^{13}\text{C}_1 > \delta^{13}\text{C}_2 < \delta^{13}\text{C}_3$ (or approximately equal to $\delta^{13}\text{C}_3$; Figure 24a). Third, the $\delta^{13}\text{C}$ of methane and ethane in the crushed gas sample is significantly enriched in ^{13}C relative to the other degassing samples. This is not surprising because the ratio of adsorbed gas to free gas should be largest in the crushed gas samples resulting in larger observed fractionations [115]. The natural gas plot for the crushed gas is like that of the most thermally mature ($\text{VR}_o \geq 4.5\%$) and marginally productive Marcellus shale-gas wells in the basin (Figure 7b).

Unlike the pressure core degassing samples, limited time-lapse geochemical analyses of Marcellus Formation natural gases in the northern Appalachian basin do not reveal significant or systematic changes of stable carbon isotope ratios that vary with production (samples noted in bold dark blue in Table 1). In the dry gas-producing region, for example, methane $\delta^{13}\text{C}$ of mud gas samples collected from the vertical and horizontal legs of the DG11/DG12 well on 2/21/2011 ranged between -25.0 and -22.8% . Methane $\delta^{13}\text{C}$ of production gas collected from the well on 10/19/2011 was -24.04% (DG11 in Table 1). Methane $\delta^{13}\text{C}$ of production gas collected on 12/18/2014 was -23.90% (DG12 in Table 1). Ethane and propane carbon isotopic data exhibit similar invariance. The $\delta^{13}\text{C}_2$ of mud gases collected on 2/21/2011 ranged between -30.3 and -28.9% and the $\delta^{13}\text{C}_3$ was between -32.6 and -30.8% . Ethane and propane $\delta^{13}\text{C}$ of production gas collected from the well on 10/19/2011 were -29.9 and -32.5% , respectively. On 12/18/2014, the production

gas $\delta^{13}\text{C}_2$ was -29.86‰ and the $\delta^{13}\text{C}_3$ was -31.4‰ . Similarly, in the wet gas-producing region, the respective methane $\delta^{13}\text{C}$ values of gas samples WG2/WG13/WG14 (same well) collected in April and May 2019 and January 2020 were -45.5 , -45.23 and -45.5‰ (Table 1). Ethane $\delta^{13}\text{C}$ of gas collected on these dates was -35.28 , -35.12 and -35.14‰ . Respective propane $\delta^{13}\text{C}$ of wet gas collected in April 2019 and in May 2019 was -30.34 and -30.34‰ . Propane $\delta^{13}\text{C}$ was -30.2 in January 2020. These observations are consistent with the model predictions of Xia and Tang [115]. Although δ value variations of up to 10‰ can occur during laboratory degassing experiments, depending on the cumulative degassing volume, production gas flowing from shale-gas reservoirs should be dominated by advective flux through stimulated fractures which has little fractionation effect [115].

4.8. Relevance to Environmental Issues in the Marcellus Play of the Appalachian Basin

In addition to energy production (heating and electricity generation), natural gas provides critical feedstock for a variety of necessities in modern economies such as basic chemicals, plastics, synthetic fibers, resins, dyes, foams, adhesives, explosives, synthetic rubber, paints and coatings, industrial chemicals, and numerous medical supplies. NGL directly contribute to the manufacture of solar panels and wind turbines. The mining of critical minerals needed to manufacture electric batteries and fuel cells is dependent on the energy supplied by fossil fuels. Natural gas extraction will continue as a fundamentally important societal resource well into the 21st Century. The Marcellus Formation in the Appalachian basin will continue to serve as one of the world's most significant natural resources for some time to come [5]. However, the commercial success of the Marcellus unconventional play has led to public apprehension about the safety of shale-gas and shale-oil extraction. Concerns about the safety of petroleum development in the region are focused on stray gas migration to shallow groundwater aquifers and wells, buildings, and the atmosphere, as well as the potential for contamination from toxic materials in produced brine or hydraulic fracturing fluid during drilling, transport, and disposal [7–10,116–120]. Hydrocarbon migration into shallow groundwater aquifers in the study area occurs both naturally [117–119,121] and as a consequence of oil and gas well operations [116,120]. The geochemical data and interpretations provided in this report comprise a significant contribution to the available regional background dataset against which stray gas investigations may be conducted [7,118,119,121].

Methane is the third most important greenhouse gas (after water vapor and CO_2) and thus an important contributor to global climate change [120]. Fossil fuels represent an obvious and important potential source of increasing atmospheric methane concentrations due to growing global production. Milkov et al. [122] utilized a global dataset of $\delta^{13}\text{C}_1$ measurements from >1600 shale-gas wells to constrain the contribution of shale-gas emissions to the observed atmospheric increases in the global CH_4 load and concluded that increases in atmospheric CH_4 since 2008 are not dominated by emissions from shale-gas operations. Their conclusions are supported by the observation that increasing CH_4 concentrations are accompanied by ^{13}C depletion. Milkov et al.'s [122] conclusions are consistent with studies by Schaefer et al. [123] and Schwietzke et al. [124] who argue that the recent increase in atmospheric CH_4 concentrations is a result of increasing microbial methane emissions with lesser to no significant increased contributions from fossil fuel emissions [125]. Howarth [126] challenged this interpretation and claimed that emissions from shale-gas, and probably shale-oil, production make up more than half of the total increase in fossil fuel emissions since 2008. He based his interpretation on the erroneous claim that the $\delta^{13}\text{C}_1$ of shale-gas is notably lighter than that of conventionally produced hydrocarbons. Lewan [125] thoroughly disputed and dismissed Howarth's [126] argument by reviewing several shale-gas datasets, including Marcellus Formation mud gas data published by Baldassare et al. [7]. The production gas isotopic dataset provided in this report support and refine the arguments of Milkov et al. [122] and Lewan [125]. The dataset for this report should also help supplement and facilitate ongoing research related to atmospheric methane and ethane emissions in the study area [10,127,128].

5. Conclusions

Regional differences in Marcellus thermal maturity and hydrocarbon alteration effects define specific wet gas and dry gas production in the Appalachian basin. Thermal maturity and hydrocarbon alteration are best constrained by fluid chemistry. Marcellus hydrocarbons recovered in the wet gas region are mixtures of residual primary-associated gases generated in the late-oil window and post-mature secondary hydrocarbons generated from oil cracking in the wet gas window. Condensate production in the wet gas region is constrained by increasing maturity in conjunction with oil cracking and gasification. Most Marcellus liquids also have been stripped by gas and altered by hydrodynamic flow and water washing. Gas stripping results in enhanced expulsion and migration in some wells resulting in reduced liquid reserves related to depletion of more volatile hydrocarbon components [129]. Water washing also removed more water-soluble compounds to varying degrees within the sample set discussed in this report. Although water washing in low permeability mudrocks may seem unlikely to many readers, several investigators have published evidence that supports this interpretation. Repetski et al. [130] speculated that a westward bulging salient in Devonian conodont alteration indices mapped in north central West Virginia reflects the migration of hot, basin-derived brines. Dorobek [131] published fluid inclusion evidence for hot basinal fluid migration through Devonian rocks in the study area. Evans [132] and Evans et al. [133] published evidence for the influx of low-salinity, CH₄-saturated brines during the Alleghenian orogeny. Tamulonis and Carter [134] recently published unequivocal evidence for hydrothermal alteration in Devonian shales in the Rome Trough. And Atwah et al. [135] documented water washing in the analogous Woodford Shale of the Anadarko basin.

Marcellus hydrocarbons recovered in the dry gas-producing region are mixtures of residual methane cracked from overmature refractory organic matter and hydrocarbons generated by extensive oil and wet gas cracking. Production in the dry gas region is largely constrained by relative gas retention versus expulsion as controlled by regional and local structure, and by seal integrity. Noble gas systematics reveal gas retention versus migration trends in the produced fluids. Thermal maturity also influences productivity where declining well performance is correlated with increasing relative proportions of late-stage residual methane and decreasing amounts of gas generated by oil/wet gas cracking. This trend is accompanied by increased aromatization, graphitization, and loss of the interconnected organic porosity within a pyrobitumen network [30] (Figure 25).

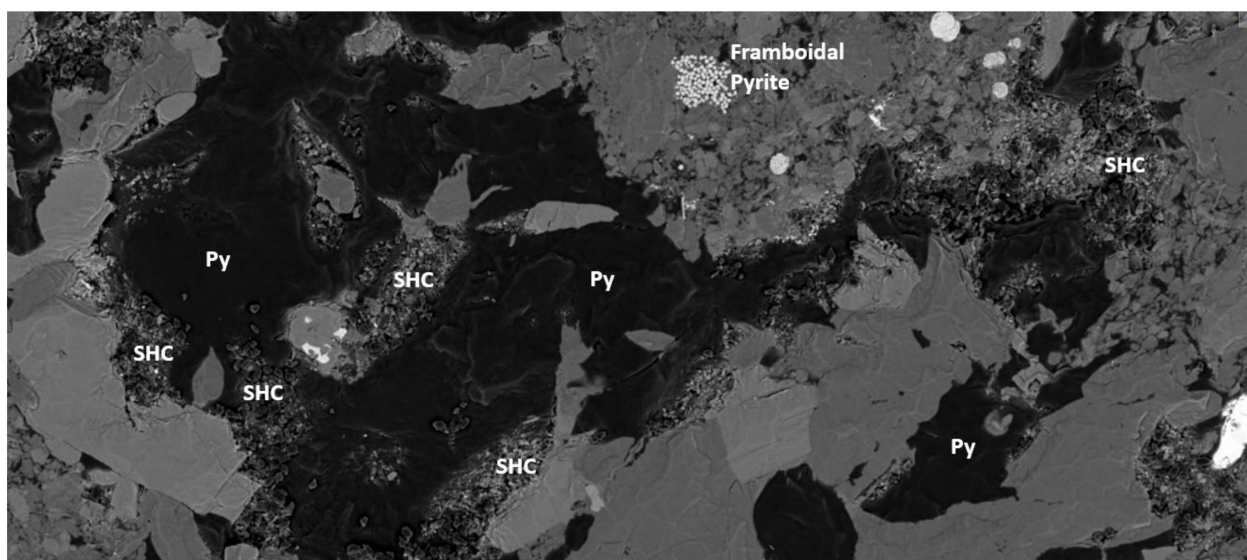


Figure 25. High-resolution large-scale mosaic of focused ion beam (FIB) BE SEM images [136] of non-productive, non-porous Marcellus shale sample from the Buda #1 well drilled in Luzerne County,

Pennsylvania. Compare with Figure 5. This SEM image is 2.2-mm-wide. TOC is as high as 8.36 wt. % (mean = 4.2 wt. %) and measured VR_o averages 3.2%. Average S_w is 72.1% of pore volume and average S_g is 21.4% of pore volume, with average gas-filled porosity only 0.8% of bulk volume. The Marcellus shale in this non-producing well contains only residual adsorbed and isotopically heavy Late-Stage CH_4 (Figure 20) due to the loss of organic-hosted pore space. The respective H/C ratio and O/C ratio of the pore-filling pyrobitumen in this sample are 0.4 and 0.06 [12]. Electron microscopy performed by Dr. Herman Lemmens, FEI.

The data provided by this report also facilitate the identification of sources of stray gas contamination and provide new baseline measurements for comparison with atmospheric greenhouse gas measurements conducted to monitor fugitive emissions of atmospheric methane.

Funding: This study was financed by Stratum Reservoir.

Data Availability Statement: Numerical data are presented in Tables 1–4. Well names and locations for the data listed in Tables 1–4 remain proprietary.

Acknowledgments: The author thanks Mark McCaffrey, Tim E. Ruble, and Matt Flannery (Stratum Reservoir) for early internal reviews of the original draft manuscript and for their encouragement and support over the course of this work. Tim Ruble in particular, and several colleagues cited in reference [12], collaborated on, debated, and co-published much of the background and ancillary data discussed in this report. The author also has benefitted from many lively discussions with Robert Burruss, Fred Baldassare, Dennis Coleman, Martin Schoell, Xinyu Xia, Yongchun Tang, Barbara Tilley, Daniel Jarvie, Stephen Brown, Wallace Dow (deceased), Michael Lewan, Thomas Darrah, Richard Drozd, and John Curtis about the origin of isotopic reversals in natural gas. The debate will continue. Wayne Knowles (Stratum Reservoir) performed and interpreted all of the organic petrographic data reported for this study. Kris Carter and John Harper (Pennsylvania Geological Survey) kindly supplied the stratigraphic diagrams in Figure 2 and their permission to publish them in this paper. William Zagorski (Range Resources) shared the SEM image in Figure 5a and provided encouragement and support for my earliest work on Marcellus Formation gases. I thank the Pennsylvania Geological Survey, Range Resources, EQT, Chief Oil and Gas, Ovintiv Inc. (formerly Encana Natural Gas), and Antero Natural Resources for permission to utilize the data provided in this report. Geochemical analyses were performed at Stratum Reservoir (formerly Weatherford Laboratories) facilities in Houston, Texas and Champaign, Illinois (Isotech Laboratories), and at SmartGas Science in Columbus, Ohio.

Conflicts of Interest: The author declares no conflict of interest.

References

1. Popova, O. *Marcellus shale play geology review*. U.S. Energy Administration Updates to Marcellus Shale Play Maps; U.S. Department of Energy: Washington, DC, USA, 2017; p. 14.
2. Higley, D.K.; Leathers-Mills, H.M.; Enomoto, C.B. Controls on petroleum resources for the Devonian Marcellus Shale in the Appalachian basin province, Kentucky, West Virginia, Ohio, Pennsylvania, and New York. *Mt. Geol.* **2019**, *56*, 323–364. [CrossRef]
3. U.S. Energy Information Administration. *Proved Reserves of Crude Oil and Natural Gas in the United States*; U.S. Energy Information Administration: Washington, DC, USA, 2022; p. 51.
4. Khosrokhavar, R.; Griffiths, S.; Wolf, K.-H. Shale-gas formations and their potential for carbon storage: Opportunities and outlook. *Environ. Process.* **2014**, *1*, 595–611. [CrossRef]
5. Carter, K.M.; Patchen, D.G. A geologic study to determine the potential to create an Appalachian storage hub for natural gas liquids. *Final. Rep. Appalach. Oil Nat. Gas. Res. Consort.* **2018**, *3*, 162.
6. Blood, D.R.; Douds, A.S.B.; Wright, M. A proposed model for quantifying critical mineral occurrence from unconventional sources: An example from the Marcellus shale, Appalachian basin, USA. In Proceedings of the 50th Annual Eastern Section AAPG Meeting Program with Abstracts, Pittsburgh, PA, USA, 3–5 October 2021; p. 19.
7. Baldassare, F.J.; McCaffrey, M.A.; Harper, J.A. A geochemical context for stray gas investigations in the northern Appalachian basin: Implications of analyses of natural gases from Neogene-through Devonian-age strata. *AAPG Bull.* **2014**, *98*, 341–372. [CrossRef]
8. Darrah, T.H.; Vengosh, A.; Jackson, R.B.; Warner, N.R.; Poreda, R.J. Noble gases identify the mechanisms of fugitive gas contamination in drinking-water wells overlying the Marcellus and Barnett Shales. *Proc. Natl. Acad. Sci. USA* **2014**, *111*, 14076–14081. [CrossRef]

9. Molofsky, L.; Connor, J.A.; Van De Ven, C.J.C.; Hemingway, M.P.; Richardson, S.D.; Strasert, B.A.; McGuire, T.M.; Paquette, S.M. A review of physical, chemical, and hydrogeologic characteristics of stray gas migration: Implications for investigation and remediation. *Sci. Total Environ.* **2021**, *779*, 146234. [CrossRef]
10. Miles, N.L.; Martins, D.K.; Richardson, S.J.; Rella, C.W.; Arata, C.; Lauvaux, T.; Davis, K.J.; Barkley, Z.R.; McKain, K.; Sweeney, C. Calibration and field testing of cavity ring-down laser spectrometers measuring CH₄, CO₂, and δ¹³CH₄ deployed on towers in the Marcellus Shale region. *Atmos. Meas. Tech.* **2018**, *11*, 1273–1295. [CrossRef]
11. Zagorski, W.A.; Wrightstone, G.R.; Bowman, D.C. The Appalachian basin Marcellus gas play: Its history of development, geologic controls on production, and future potential as a world-class reservoir. *Shale Reserv. AAPG Mem.* **2012**, *97*, 15–18.
12. Laughrey, C.D.; Lemmens, H.; Ruble, T.E.; Butcher, A.R.; Walker, G.; Kostelnik, J.; Barnes, J.; Knowles, W. Black shale diagenesis: Insights from integrated high-definition analyses of post-mature Marcellus Formation rocks, northeastern Pennsylvania. In *Critical Assessment of Shale Resource Plays*; AAPG Memoir 103; AAPG: Tulsa, OK, USA, 2013.
13. Laughrey, C.D. Produced gas and condensate geochemistry of the Marcellus Formation: Insights into petroleum maturity, migration, and alteration in an unconventional shale reservoir. URTEC Paper 5195. In Proceedings of the Unconventional Resource Technology Conference, Houston, TX, USA, 16–18 November 2020.
14. Faill, R.T. A geologic history of the north-central Appalachians; Part 2. The Appalachian basin from the Silurian through the Carboniferous. *Am. J. Sci.* **1997**, *7*, 729–761. [CrossRef]
15. Ettensohn, F.R. Controls on the development of Catskill Delta complex basin-facies. *Geol. Soc. Am. Spec. Pap.* **1985**, *201*, 65–77.
16. Beaumont, C.; Quinlan, B.; Hamilton, J. Orogeny and stratigraphy: Numerical models of the Paleozoic in the eastern interior of North America. *Tectonics* **1988**, *7*, 389–416. [CrossRef]
17. Arthur, M.A.; Sageman, B.B. Sea-level control on source-rock development: Perspectives from the Holocene Black Sea, the mid-Cretaceous western interior basin of North America, and the Late-Devonian Appalachian basin. The deposition of carbon-rich sediments: Models, mechanisms, and consequences. *SEPM Spec. Publ.* **2005**, *82*, 35–59.
18. Faill, R.T. The Acadian orogeny and the Catskill Delta. *Geol. Soc. Am. Spec.* **1985**, *201*, 15–37.
19. Ettensohn, F.R. The Catskill delta complex and the Acadian orogeny. *Geol. Soc. Am. Spec.* **1985**, *201*, 39–49.
20. Carter, K.M.; Harper, J.A.; Schmid, K.W.; Kostelnik, J. Unconventional natural gas resources in Pennsylvania: The backstory of the modern Marcellus shale play. *AAPG Bull.* **2011**, *18*, 217–257. [CrossRef]
21. Harper, J.A.; Anthony, R.V.; Carter, K.; Schmid, K.W.; Dunst, B.J.; Cooney, M. Correlation of Middle and Upper Devonian shales in the Marcellus-producing regions of Pennsylvania. In Proceedings of the Geological Society of North America Joint 52nd Northeastern Annual Section/51st North-Central Annual Section Meeting Abstracts with Programs, Pittsburgh, PA, USA, 20 March 2017; p. 49. [CrossRef]
22. Carter, K.M. Subsurface Lithostratigraphy of the Oil-and Gas-Producing Regions of Pennsylvania. Pennsylvania Geological Survey Fourth Series, Open-File Oil and Gas. Report 19-01.1; 1 Plate, 1 Appendix, and 6 Stratigraphic Cross Sections. 2019; p. 5. Available online: <https://maps.dcnr.pa.gov/publications/Default.aspx?id=985> (accessed on 22 April 2022).
23. De Witt, W., Jr.; Roen, J.B.; Wallace, L.G. *Stratigraphy of Devonian Black Shales and Associated Rocks in the Appalachian Basin*; United States Geological Survey Bulletin 1909; Reston, VA, USA, 1993.
24. Lash, G.G.; Engelder, T. Thickness trends and sequence stratigraphy of the Middle Devonian Marcellus Formation, Appalachian basin: Implications for Acadian foreland basin evolution. *AAPG Bull.* **2011**, *95*, 61–103. [CrossRef]
25. Boswell, R.; Pool, S. Lithostratigraphy of Middle and Upper Devonian organic-rich shales in West Virginia. *WVGES Rep. Investig.* **2018**, *35*, 55.
26. Sageman, B.B.; Murphy, A.E.; Werne, J.P.; Ver Straeten, C.A.; Hollander, D.J.; Lyons, T.W. A tale of shales: The relative roles of production, decomposition, and dilution in the accumulation of organic-rich strata, Middle-Upper Devonian, Appalachian basin. *Chem. Geol.* **2003**, *195*, 229–273. [CrossRef]
27. Hupp, B.N.; Donovan, J.J. Quantitative mineralogy for facies definition in the Marcellus Shale (Appalachian basin, USA) using XRD-XRF integration. *Sediment. Geol.* **2018**, *371*, 16–31. [CrossRef]
28. Root, J.C. Petrological and Isotopic Evidence for Diagenetic Evolution in the Cherry Valley Carbonates and Adjacent Mudrocks of the Marcellus ‘Shale’ from West Virginia, Pennsylvania, and New York. Master’s Thesis, Cornell University, Ithaca, NY, USA, May 2018.
29. Milliken, K.L.; Rudnicki, M.; Awwiller, D.N.; Zhang, T. Organic matter-hosted pore system, Marcellus Formation (Devonian), Pennsylvania. *AAPG Bull.* **2013**, *97*, 177–200. [CrossRef]
30. Deller Plane, C.; Bourdet, J.; Josh, M.; Clennell, M.B.; Rickard, W.D.A.; Saunders, M.; Sherwood, N.; Le, Z.; Dewhurst, D.N.; Raven, M.D. Organic matter network in post-mature Marcellus Shale: Effects on petrophysical properties. *AAPG Bull.* **2018**, *102*, 2305–2332. [CrossRef]
31. Obermajer, M.; Fowler, M.G.; Goodarzi, F.; Snowdon, L.R. Organic petrology and organic geochemistry of Devonian black shales in southwestern Ontario, Canada. *Org. Geochem.* **1997**, *26*, 229–246. [CrossRef]
32. Hackley, P.C.; Ryder, R.T. Organic geochemistry and petrology of Devonian shale in eastern Ohio: Implications for petroleum system assessment. *AAPG Bull.* **2021**, *105*, 543–573. [CrossRef]
33. Higley, D.K.; Enomoto, C.B. Burial history reconstruction of the Appalachian basin in Kentucky, West Virginia, Ohio, Pennsylvania, and New York, using 1D petroleum system models. *Mt. Geol.* **2019**, *56*, 365–3696. [CrossRef]

34. Rowan, E.L. Burial and thermal history of the central Appalachian basin based on three 2-D models of Ohio, Pennsylvania, and West Virginia. *U.S. Geol. Surv. Open-File Rep.* **2006**, *1019*, 35.
35. Bernard, B.; Brooks, J.M.; Sackett, W.M. A geochemical model for characterization of hydrocarbon gas sources in marine sediments. In Proceedings of the 9th Annual Offshore Technology Conference (OTC 2934), Houston, TX, USA, 2–5 May 1977; pp. 435–438.
36. Schoell, M. Genetic characterization of natural gases. *AAPG Bull.* **1983**, *67*, 2225–2238.
37. Golding, S.M.; Boreham, C.J.; Esterle, J.S. Stable isotope geochemistry of coal bed and shale gas and related production waters: A review. *Int. J. Coal Geol.* **2013**, *120*, 24–40. [[CrossRef](#)]
38. Milkov, A.V.; Etiope, G. Revised genetic diagrams for natural gases based on a global dataset of >20,000 samples. *Org. Geochem.* **2018**, *125*, 109–120. [[CrossRef](#)]
39. Chung, H.M.; Gormly, J.R.; Squires, R.M. Origin of gaseous hydrocarbons in subsurface environments: Theoretical considerations of carbon isotope distributions. *Chem. Geol.* **1988**, *71*, 97–103. [[CrossRef](#)]
40. Rooney, M.A.; Claypool, G.E.; Chung, H.M. Modeling thermogenic gas generation using carbon isotope ratios of natural gas hydrocarbons. *Chem. Geol.* **1995**, *126*, 219–232. [[CrossRef](#)]
41. Zumberge, J.; Ferworn, K.; Brown, S.D. Isotopic reversal (“rollover”) in shale gas produced from the Mississippian Barnett and Fayetteville formations. *Mar. Pet. Geol.* **2012**, *31*, 43–52. [[CrossRef](#)]
42. Tilley, B.; Muehlenbachs, K. Isotopic reversals and universal stages and trends of gas maturation in sealed, self-contained petroleum systems. *Chem. Geol.* **2013**, *339*, 194–204. [[CrossRef](#)]
43. Curiale, J.A.; Curtis, J.B. Organic geochemical applications to the exploration for source-rock reservoirs—A review. *J. Unconv. Oil Gas. Resour.* **2016**, *13*, 1–31. [[CrossRef](#)]
44. Pinti, D.L.; Marty, B. Noble gases in oil and gas fields: Origins and processes. In *Fluids Basin Evolution*; Mineralogical Association of Canada: Quebec, Canada, 2000; Volume 28, pp. 160–196.
45. Ballentine, C.J.; Burgess, R.; Marty, B. Tracing fluid origin, transport, and interaction in the crust. *Rev. Mineral. Geochem.* **2002**, *47*, 539–614. [[CrossRef](#)]
46. Byrne, D.J.; Barry, P.H.; Lawson, M.; Ballentine, C.J. Noble gases in conventional and unconventional petroleum systems. *Geol. Soc. Lond.* **2017**, *468*, 23. [[CrossRef](#)]
47. Ballentine, C.J.; Burnard, P.G. Production, release, and transport of noble gases in the continental crust. *Rev. Mineral. Geochem.* **2002**, *47*, 481–538. [[CrossRef](#)]
48. Podosek, F.A.; Bernatowicz, T.J.; Kramer, F.E. Adsorption of xenon and krypton on shales. *Geochim. Cosmochim. Acta* **1981**, *45*, 2401–2415. [[CrossRef](#)]
49. Marrocchi, Y.; Marty, B. Experimental determination of the xenon isotopic fractionation during adsorption. *Geophys. Res. Lett.* **2013**, *40*, 4165–4170. [[CrossRef](#)]
50. Hunt, A.G.; Darrach, T.H.; Poreda, R.J. Determining the source and genetic fingerprint of natural gases using noble gas geochemistry: A northern Appalachian basin case study. *AAPG Bull.* **2012**, *96*, 1785–1811. [[CrossRef](#)]
51. Battani, A.; Sarda, P.; Prinzhofer, A. Basin scale natural gas source, migration and trapping traced by noble gases and major elements: The Pakistan Indus basin. *Earth Planet. Sci. Lett.* **2000**, *8*, 229–249. [[CrossRef](#)]
52. Miles, J.A. *Illustrated Glossary of Petroleum Geochemistry*; Clarendon Press-Oxford: Oxford, UK, 1994; p. 137.
53. Holba, A.G.; Bone, R.L.; Huiying, B.J.; Vasquez, J.R.; Stokes, S.M. Petroleum-fluid property prediction from gas chromatographic analysis of rock extracts or fluid samples. *U. S. Pat. Appl. Publ.* **2014**, *31*, 23.
54. Adams, J.; Kornacki, A.S. Tailoring geochemical production monitoring for tight reservoirs that contain migrated oil. In Proceedings of the AAPG Hedberg Conference, The Evolution of Petroleum Systems Analysis, Houston, TX, USA, 4–6 March 2019. Available online: <https://www.searchanddiscovery.com/abstracts/html/2019/hedberg-90349/abstracts/164.html> (accessed on 22 April 2022).
55. Thompson, K.F.M. Classification and thermal history of petroleum based on light hydrocarbons. *Geochim. Cosmochim. Acta* **1983**, *11*, 573–590. [[CrossRef](#)]
56. Radke, M.; Horsfield, B.; Little, R.; Rullkötter, J. Petroleum and Basin Evolution, Chapter 3. In *Maturation and Petroleum Generation*; Welte, D.H., Horsfield, B., Baker, D.R., Eds.; Springer: Berlin/Heidelberg, Germany, 1997; pp. 169–229.
57. BeMent, W.O.; Levey, R.A.; Mango, F.D. The Temperature of Oil Generation as Defined with C₇ Chemistry Maturity Parameter (2-4-DMP/2,3-DMP Ratio). In *Organic Geochemistry: Developments and Applications in Energy, Climate, Environment, and Human History*; AIGOA: Donostia-San Sebastian, Spain, 1995; pp. 505–507.
58. Mango, F.D. The light hydrocarbons in petroleum: A critical review. *Org. Geochem.* **1997**, *26*, 417–440. [[CrossRef](#)]
59. Halpern, H.I. Development and applications of light-hydrocarbon-based star diagrams. *AAPG Bull.* **1995**, *79*, 801–815.
60. Agrawal, V.; Sharma, S. Molecular characterization of kerogen and its implications for determining hydrocarbon potential, organic matter sources, and thermal maturity in Marcellus Shale. *Fuel* **2018**, *228*, 429–437. [[CrossRef](#)]
61. Agrawal, V.; Sharma, S. Testing utility of organochemical proxies to assess sources of organic matter, paleo redox conditions, and thermal maturity in mature Marcellus shale. *Front. Energy Res.* **2018**, *6*, 42. [[CrossRef](#)]
62. Laughrey, C.D.; Baldassare, F.J. Geochemistry and origin of some natural gases in the Plateau Province, central Appalachian basin, Pennsylvania and Ohio. *AAPG Bull.* **1998**, *82*, 317–335.
63. Xia, X.; Chen, J.; Braun, R.; Tang, Y. Isotopic reversals with respect to maturity trends due to mixing of primary and secondary products in source rocks. *Chem. Geol.* **2013**, *339*, 205–212. [[CrossRef](#)]

64. Stolper, D.A.; Lawson, M.; Davis, C.L.; Ferreira, A.A.; Santos Neto, E.V.; Ellis, G.S.; Lewan, M.D.; Martini, A.M.; Tang, Y.; Schoell, M.; et al. Formation temperatures of thermogenic and biogenic methane. *Science* **2014**, *344*, 1500–1503. [[CrossRef](#)] [[PubMed](#)]
65. Whiticar, M.J. *Correlation of Natural Gases with their Sources*; AAPG Memoir 60: Tulsa, OK, USA, 1994; pp. 261–283.
66. Faber, E. Zur Isotopengeochemie gasförmiger Kohlenwasserstoffe. *Erdöl Eerdgas Kohle* **1987**, *103*, 210–218.
67. Whiticar, M.J. A geochemical perspective of natural gas and atmospheric methane. *Adv. Org. Geochem.* **1990**, *16*, 531–547. [[CrossRef](#)]
68. Clayton, C. Carbon isotope fractionation during natural gas generation from kerogen. *Mar. Pet. Geol.* **1991**, *8*, 232–240. [[CrossRef](#)]
69. Xia, X.; Tang, Y. Application of gas isotopes to the thermal history analysis of basins. *SEPM Spec. Publ.* **2012**, *103*, 147–152.
70. Prinzhofer, A.; Battani, A. Gas isotope tracing: An important tool for hydrocarbons exploration. *Oil Gas. Sci. Technol.* **2003**, *58*, 299–311. [[CrossRef](#)]
71. Kendall, C.; Caldwell, E.A. Isotope Tracers in Catchment Hydrology. In *Fundamentals of Isotope Geochemistry*; Kendall, C., McDonnell, J.J., Eds.; Elsevier: Amsterdam, The Netherlands, 1998; pp. 51–86.
72. Burruss, R.C.; Laughrey, C.D. Carbon and hydrogen isotopic reversals in deep basin gas: Evidence for limits to the stability of hydrocarbons. *Org. Geochem.* **2010**, *41*, 1285–1296. [[CrossRef](#)]
73. Harrison, M.J.; Marshak, S.; Onasch, C.M. Stratigraphic control of hot fluids on anthracitization, Lackawanna synclinorium, Pennsylvania. *Tectonophysics* **2004**, *378*, 85–103. [[CrossRef](#)]
74. Kisch, H.J.; van den Kerkhof, A.M. CH₄-rich inclusions from quartz veins in the Valley and Ridge province and the anthracite fields of the Pennsylvania Appalachians. *Am. Mineral.* **1991**, *76*, 230–240.
75. Cook, J.E.; Dunne, W.M.; Onasch, C.M. Development of a dilatant damage zone along a thrust relay in a low-porosity quartz arenite. *J. Struct. Geol.* **2006**, *28*, 776–792. [[CrossRef](#)]
76. O’Kane, A.; Onasch, C.M.; Farver, J.R. The role of fluids in low temperature fault-related deformation of quartz arenite. *J. Struct. Geol.* **2007**, *29*, 819–836. [[CrossRef](#)]
77. Onasch, C.M.; Dunne, W.M.; Cook, J.E.; O’Kane, A. The effect of fluid composition on the behavior of well cemented, quartz-rich sandstone during faulting. *J. Struct. Geol.* **2009**, *31*, 961–971. [[CrossRef](#)]
78. Lewan, M.D.; Kotarba, M.J. Thermal-maturity limits for primary thermogenic-gas generation from humic coals as determined by hydrous pyrolysis. *AAPG Bull.* **2014**, *98*, 2581–2610. [[CrossRef](#)]
79. Lewan, M.D.; Law, B.E.; Wilson, M. Fundamental Issues on Thermogenic Gas Generation from Source-Rock Maturation and Reservoir-Oil Cracking. In *Innovative Gas Exploration Concepts Symposium*; Rocky Mountain Association of Geologists: Denver, CO, USA, 2020; Volume 4.
80. Burruss, R.C. Stability and flux of methane in the deep crust—A review. *U. S. Geol. Surv. Prof. Pap.* **1993**, *1570*, 21–29.
81. Schloemer, S.; Krooss, B.M. Molecular transport of methane, ethane, and nitrogen and the influence of diffusion on the chemical and isotopic composition of natural gas accumulations. *Geofluids* **2004**, *4*, 81–108. [[CrossRef](#)]
82. Zhang, T.; Krooss, B.M. Experimental investigation on the carbon isotope fractionation of methane during gas migration by diffusion through sedimentary rocks at elevated temperature and pressure. *Geochim. Cosmochim. Acta* **2001**, *65*, 2723–2742. [[CrossRef](#)]
83. Fuex, A.N. The use of stable carbon isotopes in hydrocarbon exploration. *J. Geochem. Explor.* **1977**, *7*, 155–188. [[CrossRef](#)]
84. Jenden, P.D.; Kaplan, I.R. *Analysis of Gases in the Earth’s Crust: Final Report to the Gas*; Contract No. 5081-360-0533; National Technical Information Service Accession Number PB91-104273/XAB; Research Institute: Chicago, IL, USA, 1989.
85. Jenden, P.D.; Kaplan, I.R. Abiogenic hydrocarbons and mantle helium in oil and gas fields. *Future Energy Gases* **1993**, *1570*, 31–56.
86. Jenden, P.D.; Drazan, D.J.; Kaplan, I.R. Mixing of thermogenic natural gases in northern Appalachian basin. *AAPG Bull.* **1993**, *77*, 980–998.
87. Laughrey, C.D.; Harper, R.M. Play Obe: Upper Ordovician Bald Eagle Formation fractured anticlinal play. In *Atlas of Major Appalachian Gas Plays*; West Virginia Economical and Geologic Survey Publication V-25: Morgantown, WV, USA, 1996; pp. 164–167.
88. Sherwood Lollar, B.; Westgate, T.D.; Ward, J.A.; Slater, G.F.; Lacrampe-Couloume, G. Abiogenic formation of alkanes in the Earth’s crust as a minor source for global hydrocarbon reservoirs. *Nature* **2002**, *416*, 522–524. [[CrossRef](#)]
89. Sherwood Lollar, B.; Lacrampe-Couloume, G.; Slater, G.F.; Ward, J.A.; Moser, D.P.; Gihring, T.M.; Lin, L.-H.; Onstott, T.C. Unraveling abiogenic and biogenic sources of methane in the earth’s deep subsurface. *Chem. Geol.* **2006**, *226*, 328–339. [[CrossRef](#)]
90. Telling, J.; Lacrampe-Couloume, G.; Sherwood Lollar, B. Carbon and hydrogen isotopic composition of methane and C₂₊ alkanes in electrical spark discharge: Implications for identifying sources of hydrocarbons in terrestrial and extraterrestrial setting. *Astrobiology* **2013**, *13*, 480–483. [[CrossRef](#)]
91. Sephton, M.A.; Hazen, R.M. On the origin of deep hydrocarbons. *Rev. Mineral. Geochem.* **2013**, *75*, 449–465. [[CrossRef](#)]
92. Milkov, A.V.; Faiz, M.; Etiope, G. Geochemistry of shale gases from around the world: Composition, origins, isotope reversals and rollovers, and implications for the exploration of shale plays. *Org. Geochem.* **2020**, *143*, 103997. [[CrossRef](#)]
93. Liu, Q.; Wu, X.; Wang, X.; Jin, Z.; Zhu, D.; Meng, Q.; Huang, S.; Liu, J.; Fu, Q. Carbon and hydrogen isotopes of methane, ethane, and propane: A review of genetic identification of natural gas. *Earth-Sci. Rev.* **2019**, *190*, 247–272. [[CrossRef](#)]
94. Xia, X.; Gao, Y. Depletion of ¹³C in residual ethane and propane during thermal decomposition in sedimentary basins. *Org. Geochem.* **2018**, 121–128. [[CrossRef](#)]

95. Prinzhofer, A.; Huc, A.Y. Genetic and post-genetic molecular and isotopic fractionations in natural gases. *Chem. Geol.* **1995**, *126*, 281–290. [[CrossRef](#)]
96. Tang, Y.; Xia, X. Kinetics and mechanism of shale gas formation: A quantitative interpretation of gas isotope “rollover” for shale gas formation. In *Critical Assessment of Shale Resource Plays*; AAPG Memoir 103; AAPG: Tulsa, OK, USA, 2013.
97. Dai, J.; Xia, X.; Qin, S.; Zhao, J. Origins of partially reversed alkane $\delta^{13}\text{C}$ values for biogenic gases in China. *Org. Geochem.* **2004**, *35*, 405–411. [[CrossRef](#)]
98. James, A.T.; Burns, B.J. Microbial alteration of subsurface natural gas accumulations. *AAPG Bull.* **1984**, *68*, 957–960.
99. Krouse, H.R.; Viau, C.A.; Eliuk, L.S.; Ueda, A.; Halas, S. Chemical and isotopic evidence of thermochemical sulfate reduction by light hydrocarbons in deep carbonate reservoirs. *Nature* **1988**, *333*, 415–419. [[CrossRef](#)]
100. Thiagarajan, N.; Xie, H.; Ponton, C.; Kitchen, N.; Peterson, B.; Lawson, M.; Formolo, M.; Xiao, Y.; Eiler, J. Isotopic evidence for quasi-equilibrium chemistry in mature natural gas. *Proc. Natl. Acad. Sci. USA* **2020**, *117*, 3989–3995. [[CrossRef](#)]
101. Rowan, E.L.; Engle, M.A.; Kraemer, T.F.; Schroeder, K.T.; Hammack, R.W.; Doughten, M.W. Geochemical and isotopic evolution of water produced from Middle Devonian Marcellus shale gas wells, Appalachian basin, Pennsylvania. *AAPG Bull.* **2015**, *99*, 181–206. [[CrossRef](#)]
102. Horibe, Y.; Craig, H. D/H fractionation in the system methane-hydrogen-water. *Geochim. Cosmochim. Acta* **1995**, *59*, 5209–5217. [[CrossRef](#)]
103. Whyte, C.; Darrah, T. Integrating noble gas geochemistry to better understand hydrocarbon stable isotope reversals. AAPG Search and Discovery abstract 2019, AAPG Annual Convention and Exhibition, San Antonio, Texas, 19–22 May 2019. Available online: <https://www.searchanddiscovery.com/abstracts/html/2019/ace2019/abstracts/2180.html> (accessed on 22 April 2022).
104. Gao, L.; Schimmelmann, A.; Tang, Y.; Mastalerz, M. Isotope rollover in shale gas observed in laboratory pyrolysis experiments: Insight to the role of water in thermogenesis of mature gas. *Org. Geochem.* **2014**, *68*, 95–106. [[CrossRef](#)]
105. Osborn, S.G.; McIntosh, J.C. Chemical and isotopic tracers of the contribution of microbial gas in Devonian organic-rich shales and reservoir sandstones, northern Appalachian basin. *Appl. Geochem.* **2010**, *25*, 456–471. [[CrossRef](#)]
106. Gao, D.; Shumaker, R.C.; Wilson, T.H. Along-axis segmentation and growth history of the Rome Trough in the central Appalachian basin. *AAPG Bull.* **2000**, *84*, 75–99.
107. Curtis, J.; Faure, G. Accumulation of organic matter in the Rome Trough of the Appalachian basin and its subsequent thermal history. *AAPG Bull.* **1997**, *81*, 424–437.
108. Roden, M.K.; Miller, D.S. Apatite fission-track thermochronology of the Pennsylvania Appalachian basin. *Geomorphology* **1989**, *2*, 39–51. [[CrossRef](#)]
109. Laughrey, C.D.; Billman, D.A.; Canich, M.R. Petroleum geology and geochemistry of the Council Run gas field, north central Pennsylvania. *AAPG Bull.* **2004**, *88*, 213–239. [[CrossRef](#)]
110. Glick, E.V. Connectivity of the Oriskany Sandstone with the Marcellus Shale: Effects on Shale-Gas Operations in North Central Pennsylvania. Master’s Thesis, University of Pittsburgh, Pittsburgh, PA, USA, 2017.
111. Laughrey, C.D.; Baldassare, F.J. Petroleum Geochemistry of Devonian Rocks and Produced Oil and Natural Gas in the Caseman-Gross Unit #1 Well, Bradford County, Pennsylvania. AAPG Search and Discovery Abstract. 2016. Available online: <https://www.searchanddiscovery.com/abstracts/html/2016/90258es/abstracts/1.50.html> (accessed on 11 May 2022).
112. Turner, A.C.; Korol, R.; Eldridge, D.L.; Bill, M.; Conrad, M.E.; Miller, T.F.; Stolper, D.A. Experimental and theoretical determinations of hydrogen isotopic equilibrium in the system $\text{CH}_4\text{-H}_2\text{-H}_2\text{O}$ from 3 to 200 °C. *Geochim. Cosmochim. Acta* **2021**, *314*, 223–269. [[CrossRef](#)]
113. Niemann, M.; Whiticar, M.J. Stable isotope systematics of coalbed gas during desorption and production. *Geosciences* **2017**, *7*, 43. [[CrossRef](#)]
114. Mahzari, P.; Mitchell, T.M.; Jones, A.P.; Westacott, D.; Striolo, A. Direct gas-in-place measurements prove much higher production potential than expected for shale formations. *Nat. Sci. Rep.* **2021**, *11*, 10775. [[CrossRef](#)]
115. Xia, X.; Tang, Y. Isotope fractionation of methane during natural gas flow with coupled diffusion and adsorption/desorption. *Geochim. Cosmochim. Acta* **2012**, *77*, 489–503. [[CrossRef](#)]
116. Osborn, S.G.; Vengosh, A.; Warner, N.R.; Jackson, R.B. Methane contamination of drinking water accompanying gas-well drilling and hydraulic fracturing. *Proc. Natl. Acad. Sci. USA* **2011**, *108*, 172–178. [[CrossRef](#)]
117. Warner, N.R.; Jackson, R.B.; Darrah, T.H.; Osborn, S.G.; Down, A.; Zhao, K.; White, A.; Vengosh, A. Geochemical evidence for possible natural migration of Marcellus Formation brine to shallow aquifers in Pennsylvania. *Proc. Natl. Acad. Sci. USA* **2012**, *109*, 11961–11966. [[CrossRef](#)]
118. Darrah, T.H.; Jackson, R.B.; Vengosh, A.; Warner, N.R.; Whyte, C.J.; Walsh, T.B.; Kondash, A.J.; Poreda, R.J. The evolution of Devonian hydrocarbon gases in shallow aquifers in the northern Appalachian basin: Insights from integrating noble gas and hydrocarbon chemistry. *Geochim. Cosmochim. Acta* **2014**, *170*, 321–355. [[CrossRef](#)]
119. Molofsky, L.J.; Connor, J.A.; Wylie, A.S.; Wagner, T.; Farhat, S.K. Evaluation of methane sources in groundwater in northeastern Pennsylvania. *Groundwater* **2018**, *51*, 333–349. [[CrossRef](#)]
120. Hammond, P.A.; Wen, T.; Brantley, S.L.; Engelder, T. Gas well integrity and methane migration: Evaluation of published evidence during shale-gas development in the USA. *Hydrol. J.* **2020**, *28*, 1481–1502. [[CrossRef](#)]
121. Reese, S.O.; Neboga, V.V.; Pelepko, S.; Kosmer, W.J.; Beattie, S. Groundwater and petroleum resources of Sullivan County, Pennsylvania. *Pa. Geol. Surv. Fourth Ser. Water Resour. Rep.* **2014**, *71*, 142.

122. Milkov, A.V.; Schwietzke, S.; Allen, G.; Sherwood, O.; Etiope, G. Using global isotopic data to constrain the role of shale gas production in recent increases in atmospheric methane. *Nat. Res. Sci. Rep.* **2020**, *10*, 4199. [[CrossRef](#)]
123. Schaefer, H.; Mikaloff-Fletcher, S.E.; Veidt, C.; Lassy, K.R.; Brailsford, G.W.; Bromley, T.M.; Dlubokencky, E.J.; Michel, S.E.; Miller, J.B.; Levin, I.; et al. A 21st Century shift from fossil-fuel to biogenic methane emissions indicated by $^{13}\text{CH}_4$. *Science* **2016**, *352*, 80–84. [[CrossRef](#)]
124. Schwietzke, S.; Sherwood, O.; Bruhwiler, L.M.P.; Miller, J.B.; Etiope, G.; Dlubokencky, E.J.; Michel, S.E.; Arling, V.A.; Vaugn, B.H.; White, J.W.C.; et al. Upward revision of global fossil fuel methane emissions based on isotope database. *Nature* **2016**, *538*, 88–91. [[CrossRef](#)]
125. Lewan, M.D. Comments on “Ideas and perspectives: Is shale-gas a major driver of recent increase in global atmospheric methane?” by Robert, W. Howarth (2019). *Biogeosci. Discuss.* **2020**. preprint. [[CrossRef](#)]
126. Howarth, R.W. Ideas and perspectives: Is shale-gas a major driver of recent increase in global atmospheric methane? *Biogeosciences* **2019**, *16*, 3033–3046. [[CrossRef](#)]
127. Barkley, Z.R. Estimating methane emissions from underground coal and natural gas production in southwestern Pennsylvania. *Geophys. Res. Lett.* **2019**, *46*, 4531–4540. [[CrossRef](#)]
128. Barkley, Z.R.; Davis, K.J.; Feng, S.; Cui, Y.Y.; Fried, A.; Weibring, P.; Richter, D.; Walega, J.G.; Miller, S.M.; Eckl, M.; et al. Analysis of oil and gas ethane and methane emissions in the southcentral and eastern United States using four seasons of continuous aircraft ethane measurements. *J. Geophys. Res. Atmos.* **2021**, *126*, e2020JD034194. [[CrossRef](#)]
129. Smith, C.; Pool, S.; Dinterman, P.; Moore, J.; Vance, T.; Smith, T.; Gordon, P.; Smith, M. Evaluating the liquids potential and distribution of West Virginia’s Marcellus liquids fairway. In Proceedings of the URTEC Paper 5540 Unconventional Resource Technology Conference, Houston, TX, USA; 2020; p. 22.
130. Repetski, J.E.; Ryder, R.T.; Avary, K.L.; Trippi, M.H. Thermal maturity patterns (CAI and %R_o) in the Ordovician and Devonian rocks of the Appalachian basin in West Virginia. *USGS Open File Rep.* **2005**, *1078*, 69.
131. Dorobek, S. Migration of orogenic fluids through the Silurio-Devonian Helderberg Group during late Paleozoic deformation: Constraints on fluid sources and implications for thermal histories of sedimentary basins. *Tectonophysics* **1989**, *159*, 25–45. [[CrossRef](#)]
132. Evans, M.A. Fluid inclusions in veins from the Middle Devonian shales: A record of deformation conditions and fluid evolution in the Appalachian Plateau. *Geol. Soc. Am. Bull.* **1995**, *107*, 327–339. [[CrossRef](#)]
133. Evans, M.A.; Battles, D.A. Fluid inclusion and stable isotope analyses of veins from the central Appalachian Valley and Ridge Province: Implications for regional synorogenic hydrologic structure and fluid migration. *Geol. Soc. Am. Bull.* **1999**, *111*, 1841–1860. [[CrossRef](#)]
134. Tamulonis, K.L.; Carter, K.M. Evidence of hydrothermal alteration in Devonian shales from the Eastern Gas Shales Project 2 core of the Rome Trough, Appalachian basin, United States. *AAPG Bull.* **2021**, *28*, 1–24. [[CrossRef](#)]
135. Atwah, I.; Sweet, S.; Pantano, J.; Knap, A. Light hydrocarbon geochemistry: Insight into Mississippian crude oil sources from the Anadarko basin, Oklahoma, USA. *Geofluids* **2019**, *2019*, 2795017. [[CrossRef](#)]
136. Lemmens, H.; Richards, D. Multiscale Imaging of Shale Samples in the Scanning Electron Microscope. *Electron Microsc. Shale Hydrocarb. Reserv. AAPG Mem.* **2013**, *102*, 27–35.